Materials Advances

REVIEW

View Article Online
View Journal | View Issue

Cite this: *Mater. Adv.*, 2021, 2, 5300

Recent advances in simulating gas permeation through MOF membranes

Hilal Daglar, [a] Ilknur Erucar [b] and Seda Keskin *[a]

Received 11th January 2021,
Accepted 21st July 2021

DOI: 10.1039/d1ma00026h

rsc.li/materials-advances

In the last two decades, metal organic frameworks (MOFs) have gained increasing attention in membrane-based gas separations due to their tunable structural properties. Computational methods play a critical role in providing molecular-level information about the membrane properties and identifying the most promising MOF membranes for various gas separations. In this review, we discuss the current state-of-the-art in molecular modeling methods to simulate gas permeation through MOF membranes and review the recent advancements. We finally address current opportunities and challenges of simulating gas permeation through MOF membranes to guide the development of high-performance MOF membranes in the future.

1. Introduction

Membrane-based gas separation has environmental and economic advantages due to its renewable and continuous operation, and low energy consumption.[1] Membranes today have several industrially important gas separation applications such as nitrogen separation from air (O_2/N_2), natural gas purification (CO_2/CH_4, H_2S/CH_4, He/CH_4), hydrogen recovery (H_2/N_2, H_2/CH_4, H_2/CO), and recovery of light olefins (C_3H_6/N_2, C_2H_4/N_2, C_2H_4/Ar, CH_4/N_2).[2] The membrane selectivity and gas permeability (or permeance) are the key parameters to describe the performance of a membrane. Although the commercial market is currently dominated by polymeric membranes due to their scalability and low cost,[3] they possess a trade-off between selectivity and gas permeability.[4,5] There has been continuous efforts for developing new membrane materials that can offer both high gas permeability and high gas selectivity for different types of gas separation processes.

For the last two decades, metal organic frameworks (MOFs), which are composed of inorganic metal nodes linked by organic linkers, have been known as an exciting class of porous materials.[6] MOFs are studied in many different fields such as catalysis,[7] optics,[8] sensing,[9] adsorption,[10] liquid[11] and gas separation[12] due to their exceptional chemical and physical properties. Among these fields, MOFs have been widely used in gas adsorption and separation applications since structural features such as high porosities, large surfaces areas, and tunable shape-selective pore sizes make them highly efficient for gas separation. Both thin-film MOF membranes and MOF-based mixed matrix membranes (MMMs) where MOFs are used as fillers in a polymer matrix are studied for gas separations. Since fabricating scalable and defect-free thin-film MOF membranes is challenging, MOF-based MMMs offer the advantages of easy processability of polymers and low-cost manufacturing process for industrial gas separations. Several excellent reviews in the literature summarize experimental fabrication and applications of thin-film MOF membranes and MOF-based MMMs.[13–19]

Thanks to the existence of various types of organic and inorganic building blocks, the number of synthesized MOFs available in the Cambridge Structural Database (CSD)[20] is dramatically increasing in each year and more than 100 000 MOFs have been already reported. Performing experiments for each MOF to assess its desired gas separation performance is highly challenging since fabrication of thin-film MOF membranes, characterizing membrane structures, and further measurements of gas permeation through the pores of new MOF membranes require long times, extensive efforts and sources. Therefore, computational studies, especially high-throughput screening studies, play a significant role in assessing the performance of MOF membranes in a reasonable time in addition to providing molecular-level understanding of gas permeation in MOFs.[21] By using molecular simulations, it is possible to quickly and accurately assess the potential of a MOF membrane for many different gas separations and under different operational conditions which may not be easily achieved by experiments.[22] Using the key performance metrics, one can computationally screen MOFs and identify the best performing membranes to direct the experimental efforts, time and sources to these potential candidates. Thus, the membrane community

[a] *Department of Chemical and Biological Engineering, Koc University, Rumelifeneri Yolu, Sariyer, 34450, Istanbul, Turkey. E-mail: skeskin@ku.edu.tr; Tel: +90-(212)-338-1362*
[b] *Department of Natural and Mathematical Sciences, Faculty of Engineering, Ozyegin University, Cekmekoy, 34794, Istanbul, Turkey*

significantly benefits from the high-quality computer simulations not only for unlocking the performance of existing MOFs but also for the discovery of new MOF membranes.

In this review, we first introduce the current state-of-the-art for the computational approaches used to simulate gas permeation through MOF membranes. We then discuss the representative examples from the literature to reveal the recent achievements in modeling MOF membranes and finally address both the opportunities and challenges of these computational methods to provide some guidelines for future studies.

2. Computational methods for predicting gas permeation

Fig. 1 represents computational methodologies commonly followed to compute gas permeation through MOF membranes. In high-throughput computational screening, MOFs are generally taken from material databases such as CSD MOF subset,[23] the computation-ready experimental (CoRE) MOF[24] database and hypothetical (computer generated) MOF database.[25] As shown in Fig. 1(a), structural properties of MOFs such as surface areas, pore sizes, pore volumes, and densities are first calculated and used to refine the number of MOFs to be studied. For example, if one wants to identify the promising MOF membranes for H_2/CO_2 separation, discarding MOFs with pore sizes less than 3.3 Å will be useful to narrow down the materials space so that both H_2 (2.8 Å) and CO_2 (3.3 Å) molecules can pass through the membrane's pores. It is important to note that pore size screening can be done to obtain molecular sieving membranes where one type of gas passes through the pores whereas the others do not.[26–28] Although the selectivity of molecular sieving membranes such as zeolite imidazolate framework-7 (ZIF-7) was measured to be very high, gas permeability was generally quite low due to the narrow pores.[29] Therefore, MOFs with pore sizes larger than the size of the largest gas molecule can be more preferable to achieve both high selectivity and high permeability. After the selection of appropriate MOFs for a given membrane-based gas separation, molecular simulations can be performed to investigate gas adsorption and diffusion properties of MOFs.

In molecular simulations, the intermolecular interactions (between gas-gas and MOF-gas) are described with van der Waals (vdW) and electrostatic interactions. Several potentials in different level of accuracy such as Morse,[30] Mie[31] and Buckingham[32] can be used to compute intermolecular interactions in molecular simulations. Among these, Lennard-Jones 12-6 (LJ)[33] and Coulomb[34] potentials are the most popular to define repulsion–dispersion forces in vdW interactions and electrostatic interactions, respectively. LJ parameters of MOFs are commonly taken from the generic force fields such as the Universal Force Field (UFF)[35] and DREIDING.[36] On the other hand, complex interactions such as the ones between gases and open metal sites of MOFs and structural flexibility of MOFs may require highly accurate force fields such as MOF-FF[37] and BTW-FF.[38] Several studies showed that although generic force fields are not enough to accurately identify some specific interactions between gas and MOFs' atoms, these force fields generally give reasonable results in high-throughput screening studies.[39,40] We also previously showed that simulated data of MOFs obtained with generic force fields such as DREIDING and UFF agree well with those of experimentally tested MOFs for several gas separations such as H_2/CH_4,[41] CO_2/N_2,[42,43] H_2/CO_2,[44] CO_2/CH_4,[42] He/CH_4[45] and C_2H_6/C_2H_4.[46] A variety of gas models can

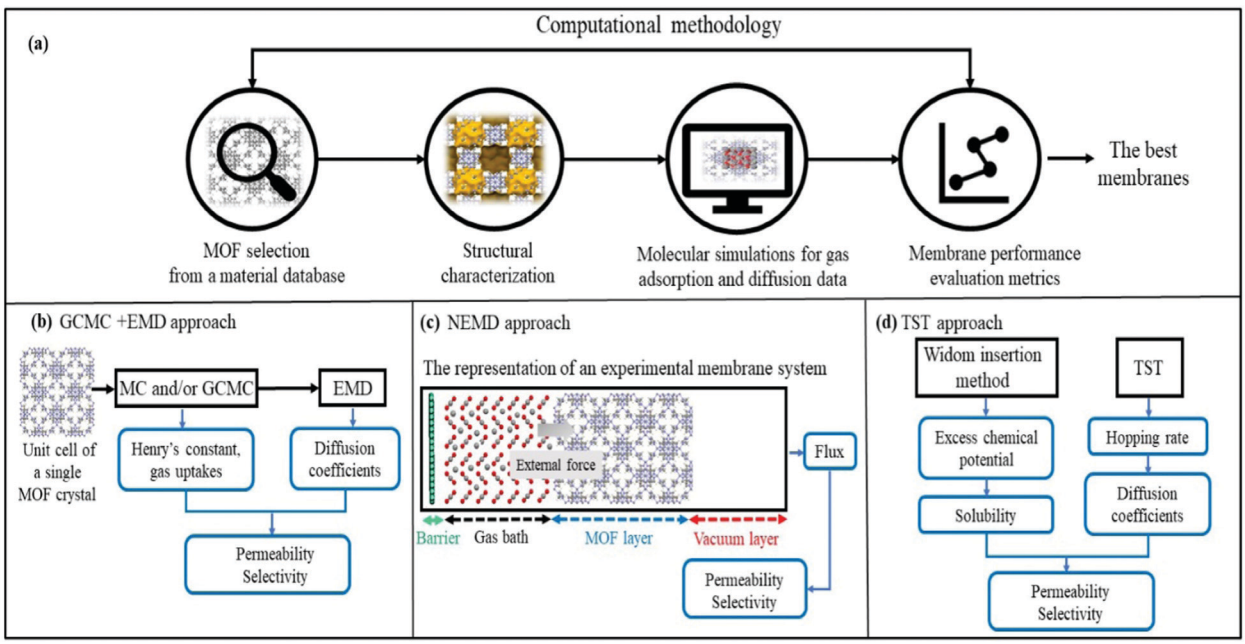

Fig. 1 Schematic comparison of computational methodologies to predict gas permeation through MOF membranes: (a) high-throughput computational screening methodology, (b) GCMC + EMD approach, (c) NEMD approach and (d) TST approach.

be used to obtain LJ parameters for gases. For example, TraPPE[47] is generally used for CH_4 which is considered as single-spherical and nonpolar atoms. Five-site model[48] is also used for CH_4, and it was shown that the single-site model leads to higher gas uptake compared to the results obtained from simulations with the five-site model of CH_4.[49] Similar to TraPPE model, Buch model[50] assumes a single-site and spherical nonpolar atom, and commonly used for H_2. However, single-site H_2 model can fail to yield accurate gas uptake predictions at low temperature ($\sim$77 K) due to the quantum effects. Yang *et al.*[51] used two-site model for H_2 adsorption and showed that H_2 uptakes in IRMOF-1 and IRMOF-18 obtained by using two-site model show better agreement with the experimental measurements of H_2 uptake at 77 K. Apart from two-site model, a three-site model with diatomic molecule and a dummy atom at the center of mass, is also used for H_2 to consider the quadratic Feynman-Hibbs (FH) effective potential.[52] EPM2,[53] a linear and three-site model, is commonly used for CO_2 molecule. Similarly, a three-site model including a dummy atom at the center of mass is used for O_2[54] and N_2.[55] Adatoz and Keskin[56] showed the accuracy of the gas models (single-site model for CH_4 and H_2, EPM2 for CO_2 and three-site model of N_2) by comparing the gas permeance predictions with the experimental measurements for eight common MOFs (IRMOF-1, Ni-MOF-74, MIL-53(Al)), and a family of ZIFs (-8, -69, -78, -90, and -95) using GCMC + EMD approach. A good agreement between predicted pure and mixture gas permeances of these MOFs and experimental measurements was reported.

To compute the electrostatic interactions, partial point charges of MOFs are assigned using either a quick charge estimation method such as charge equilibration method (Q_{eq})[57] or a more accurate DFT-based but computationally costly method such as density derived electrostatic and chemical (DDEC),[58] charges from electrostatic potentials using a grid (CHELPG)[59] and repeating electrostatic potential extracted atomic charge (REPEAT)[60] methods. We previously compared DDEC and Q_{eq} methods for CO_2/CH_4 separation performances of 1500 MOFs and showed that the selection of charge method can quantitatively affect the performances of MOFs but it does not significantly change the ranking of MOFs based on different performance metrics such as regenerability and adsorbent performance score in a high-throughput computational screening study.[61]

To examine the gas permeation through MOF membranes, the solution-diffusion model[62,63] which considers the solubility and mobility of gas molecules in dense membranes is widely used. Since MOFs have permanent pores and the solubility term is based on gas adsorption within these pores, we refer to this model as ''sorption-diffusion''. To compute the permeability of gas molecules, two common computational approaches, GCMC + EMD (Fig. 1(b)) and NEMD (Fig. 1(c)) are used. In the first method (GCMC + EMD), the membrane system is mimicked by using the unit cell of single MOF crystals rather than using a real membrane system as shown in Fig. 1(b). Here, MOF crystal is represented by defect-free and continuous single crystallographic unit cell with no grain boundaries. Henry's constants of different gases (K_i^0 and K_j^0) for adsorption are calculated by performing Monte Carlo (MC) simulations at zero-coverage by the Widom particle insertion method.[64] In this method, a ghost particle is inserted to consider only the interactions between gas and framework atoms. It is important to note that since GCMC + EMD approach assumes that the molar volume of the fluid in the membrane phase is the same with the one exists in the bulk phase, this method is more reliable when different gases in the mixture do not have a strong interaction with each other at low pressures.[65] Single-component self-diffusivities (D_i^0, D_j^0) of gases i and j are then calculated by performing equilibrium molecular dynamics (EMD) simulations at infinite dilution. Gas-gas intermolecular interactions are generally switched-off in EMD simulations to mimic infinite dilution. We note that there is generally an inverse relationship between the adsorption and diffusion properties of gases since strongly adsorbed gas molecules (having high affinity to the framework atoms) generally diffuse slower than the weakly adsorbed ones.[43] Gas permeability of MOFs (P_i^0) at infinite dilution is estimated as the multiplication of adsorption (mol kg^{-1} Pa^{-1}) and diffusion (m^2 s^{-1}) terms which are directly obtained from MC and EMD simulations:

$$P_i^0 = K_i^0 \times D_i^0 \quad (1)$$

Self-diffusivities can be computed from the mean square displacement of a tagged particle by using Einstein relation.[66] At non-dilute adsorbate loadings, both self- and corrected diffusivities can be obtained from EMD simulations. While self-diffusivities identify the motion of one tagged gas molecule in the framework, corrected diffusivities describe the collective motion of multiple adsorbed gas molecules. To compute single-component gas permeability by using the corrected diffusivities, transport (Fickian) diffusivity (D_t) is defined as the multiplication of corrected diffusivity and thermodynamic correction factor including concentration (c) and partial pressure (f):

$$D_t(c) = D_0(c)\left(\frac{\partial \ln f}{\partial \ln c}\right)_T \quad (2)$$

We note that self- and transport diffusivities of gases for MOFs differ at high loadings. For example, Skoulidas and Sholl[67] showed that self- and transport diffusivities of Ar, CH_4, CO_2, N_2 and H_2 in MOF-5 are similar at infinite dilution whereas the diffusion coefficients are found to be different at high concentration. They also showed that while self-diffusivities of gases in MOF-5 are inversely proportional to the gas loading, transported diffusivities enhance with the increase in gas loading. More detailed discussion for comparison of transport and self-diffusivities can be found in previous papers.[68,69] Gas flux, J_i, (mol m^{-2} s^{-1}) can be then calculated using transport diffusivity (m^2 s^{-1}) and concentration gradient (mol m^{-4}) in Fick's law as follow:

$$J_i = -D_t(c)\nabla c \quad (3)$$

Gas permeability, P_i, (mol m^{-1} s^{-1} Pa^{-1}) is then calculated by using the gas flux, membrane thickness, L_x, (m) and the partial pressure drop, Δf_i, (Pa) of the gas species as follows:

$$P_i = \frac{J_i}{\Delta f_i / L_x} \quad (4)$$

Gas permeability is generally reported in "Barrer". Mixture gas permeabilities (P_i^{mix}) are calculated using the concentration of the gas at the upstream face of the membrane, c_i^{mix}, (mol m^{-3}) obtained from the GCMC simulations at a specified pressure and gas diffusivities obtained from the EMD simulations, D_i^{mix}, (m^2 s^{-1}) based on the partial pressures of gases in the mixture, f_i, (Pa) as follows:

$$P_i^{mix} = \frac{c_i^{mix} \times D_i^{mix}}{f_i} \quad (5)$$

We note that adsorbed gas loadings taken from GCMC simulations are used as the input of EMD simulations. Specifically, the atomic coordinates of adsorbed gas molecules are defined at the initialization step in EMD simulations. In addition to the GCMC + EMD and NEMD approaches, transition state theory (TST)[70] can be used to compute diffusion properties of gases and TST approach has been used to compute membrane properties of MOFs as shown in Fig. 1(d) in several studies.[71–73] In this approach, adsorption properties of MOFs are computed with the Widom particle insertion method.[74] A single gas molecule is inserted into the MOF's pores and the energy between MOF atoms and gas molecule is computed. By using the intermolecular energy, U^{inter}, (J), and the thermodynamic beta, β, (J^{-1}), the excess chemical potential, μ^{ex}, (J mol^{-1}) is obtained as follows:

$$\mu^{ex} = -\frac{1}{\beta} \times \ln\left[\exp\left(-\beta \times U^{inter}\right)\right] \quad (6)$$

The gas solubility, S, (cm^3 (STP) J^{-1}) is then calculated by using μ^{ex}:

$$S_i = \frac{22\,400\ \text{cm}^3\ (\text{STP})}{\text{mol}} \times \frac{1}{RT} \exp\left(-\frac{\mu^{ex}}{RT}\right) \quad (7)$$

In TST approach, diffusion is described as successful hopping rates of a molecule from one cage to the adjacent cages. Hopping rate is also multiplied with a correction factor considering the failure thermalization to the new state after the successful jump of the gas molecules which is called dynamically corrected TST.[75] By using the hopping (exiting) rate, diffusivity of a single gas molecule (D_0) is computed as follows:

$$D_{0,i} = \frac{1}{2n} k_{EXIT} l^2 \quad (8)$$

where k_{EXIT} is the exiting rate, l is the length of jump of gas molecule (hopping distance between two neighboring cages) and n is the dimensionality of diffusion. To compute gas permeability, gas solubility and diffusivity are multiplied as follows:

$$P_i = D_{0,i} \times S_i \quad (9)$$

Membrane selectivity ($S_{i/j}^{mem}$) is then calculated as the ratio of permeability of different gas pairs (i and j).

$$S_{i/j}^{mem} = \frac{P_i^0}{P_j^0}, S_{i/j}^{mem} = \frac{P_i}{P_j}, S_{i/j}^{mem} = \frac{P_i^{mix}}{P_j^{mix}} \quad (10)$$

Selectivity of a MOF membrane can be dominated by either equilibrium-based selectivity or kinetic-based selectivity depending on the MOF-gas interactions. The former is attributed to the thermodynamic selectivity (or adsorption selectivity) and it can be defined as the separation efficiency based on the adsorbed gas amounts and their adsorption heats at equilibrium whereas the kinetic-based selectivity is considered as shape selectivity (or diffusion selectivity) and the separation efficiency is based on transport properties of gas molecules through the pores of the membrane.

Non-equilibrium molecular dynamics (NEMD) simulations are performed by constructing a more realistic representation of the membrane system. Fig. 1(c) shows a typical computational membrane system, which is constructed by gas bath, MOF and vacuum layers to perform NEMD simulations. An external force is generally applied for introducing a pressure gradient for gas molecules considering permeate and retentate sides of the membrane and feed depletion problem can be tackled using this external force. Due to periodicity of the unit cell, the pressure gradient between gas bath and vacuum layer can cause the gas molecules to escape towards vacuum layer. Therefore, as shown in Fig. 1(c), a physical barrier such as graphene layer before gas bath is required.[76] The interaction between gas molecules and the physical barrier should be switched off to eliminate the effect of physical barrier on membrane gas separation. NEMD simulations consider mass transfer resistance, which is a resistance on membrane surface caused by the diffusion of gases through membrane pores.[77,78] High mass transfer resistance on the membrane surface can lead to the blockage of the membrane pores and diminishes permeability and membrane selectivity.[79] For example, Wenk *et al.*[80] showed that mass transfer coefficient for O_2 in a polymeric membrane decreases as the membrane thickness increases. Although the thickness of experimentally tested MOF membranes is higher than the computationally simulated ones, the thickness of MOF membranes is taken as approximately 40–50 Å in computational studies to save computational time.[81–83] Therefore, considering mass transfer resistance in simulations is important to mimic the real gas separation unit. Different than the GCMC + EMD approach, membrane properties are directly computed from NEMD simulations. The amount of gas molecules transported through the unit area of MOF membrane per unit simulation time can be calculated as gas flux (J_i). Gas permeability (P_i) is then calculated by using eqn (4) as we mentioned above.

In the literature, although a variety of techniques to consider non-equilibrium conditions in MD simulations has been used to make more accurate representation of a membrane system,[84–86] the number of studies on NEMD simulations to estimate gas permeation through MOFs is limited. The most important reason is that performing NEMD simulations takes considerably longer times for getting membrane properties of MOFs compared to performing GCMC + EMD simulations, which promotes GCMC + EMD approach especially in high-throughput computational screening studies as we discuss below.

So far, we focused on modelling of pure MOF membranes for gas separation. MOFs can be also used as filler particles incorporated into polymers to improve gas permeability and selectivity of polymers. Fig. 2 shows two different methods used

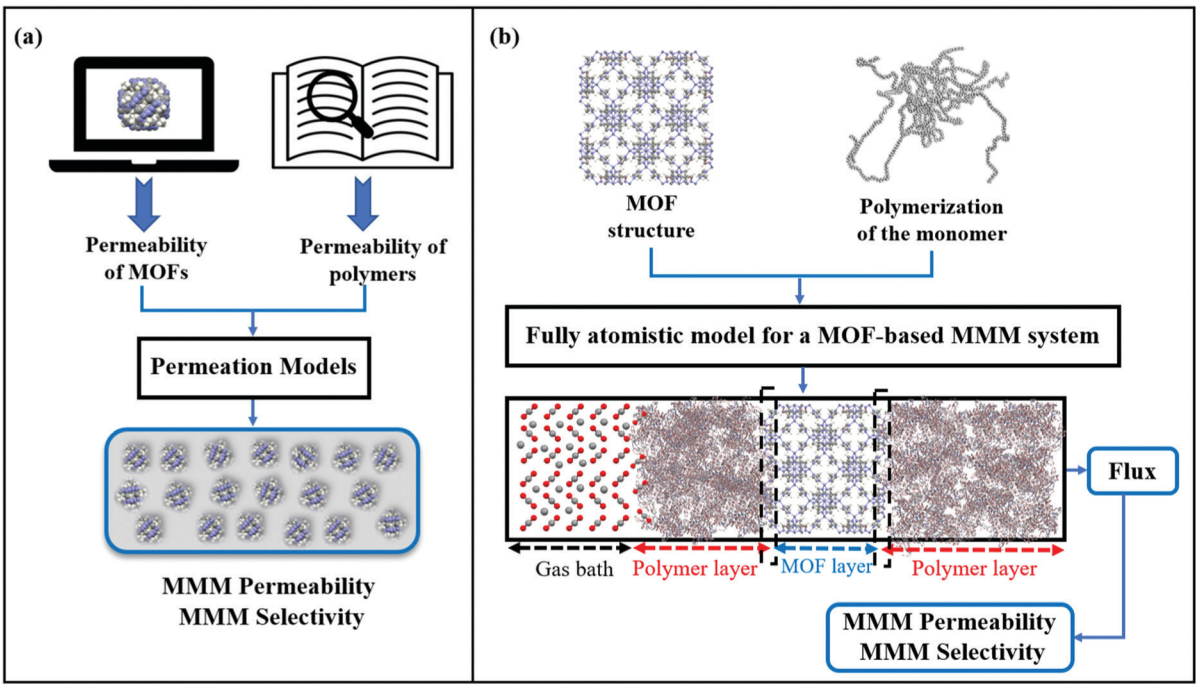

Fig. 2 Schematic comparison of computational methodologies to predict gas permeation through MOF-based MMMs: (a) combination of atomistic and continuum modeling, (b) fully atomistic approach. Dash line in (b) represents the MOF-polymer interface.

in computational studies to estimate selectivity and gas permeability of MOF-based MMMs. In the first method known as combination of atomistic and continuum modeling, gas permeabilities of MOFs are obtained from atomic simulations and permeability of MOF-based MMMs are estimated by using a theoretical permeation model (Bruggeman,[87] Pal,[88] Felske,[89] and Maxwell[90] *etc.*) as shown in Fig. 2(a). When these models are used, gas permeability data of polymer is generally obtained from the single-component gas measurements available in the literature. For example, in Maxwell model, permeability of MMM is dependent on the volume fraction of MOF filler (ϕ) and permeabilities of pure polymer (P^{P}) and pure MOF (P^{MOF}) as follows:

$$P^{MMM} = P^{P} \times \left[\frac{2 \times (1-\phi) + (1+2\phi) \times \left(P^{MOF}/P^{P}\right)}{(2+\phi) + (1-\phi) \times \left(P^{MOF}/P^{P}\right)}\right] \quad (11)$$

Since defect-free and rigid MOF assumptions are generally used in molecular simulations, representation of MMM morphologies depends on the selection of theoretical permeation models. For example, Maxwell model assumes ideal MMMs where MOF particles are perfectly dispersed in a polymer matrix and no defects in the polymer-particle interface are observed whereas Felske model accounts for non-ideal morphologies which include interface voids and polymer rigidification around particles. We previously showed that using Maxwell model among the theoretical models based on the ideal morphology and the modified Felske model among the ones considering interfacial morphology make accurate predictions for gas permeation through MOF-based MMMs.[91]

In the second method referred as the fully atomistic approach (Fig. 2(b)), both polymer and MOF are atomically modelled and the effects of interface interactions on properties of MOF-based MMMs are considered in simulation. In this method, three main steps are generally followed: (i) equilibration of the selected monomer chains with various EMD simulation steps at several *NVT* and *NPT* ensembles to reach the desired density of a polymer, (ii) combining polymer and MOF surfaces having the lowest surface energy within the same simulation box, (iii) performing several EMD runs for equilibration of the MMM. This method is nontrivial since creating a proper polymer matrix and considering the appropriate model for MOF/polymer interface is computationally costly. After constructing a fully atomistic representation of MOF-based MMMs, either GCMC + EMD or NEMD simulations can be used to predict properties of MMMs.[92,93] We note that in fully atomistic simulations, considering the structural flexibility of MOFs and interfacial interactions between MOF surfaces and polymers is important since these interactions play a significant role in identifying MOF/polymer interface compatibility.[93,94]

3. Simulated membrane properties of MOFs

Achieving high gas purity using polymer membranes is still challenging. For example, polymers only have ~10% commercial use for the natural gas purification due to their low CO_2 permeability and low CO_2/CH_4 selectivity.[2] Since polymers dominate the current market, outperforming the performance of polymers is the primary goal of developing new membranes for industrial use.

With the development of efficient MOF membranes and MOF-based MMMs, high separation performance can be achieved for various gas pairs.

We compare the performance of MOF membranes and MOF-based MMMs with that of polymers in Fig. 3 by collecting all the experimental and computational data available in the literature for three important gas separations, CO_2/CH_4, CO_2/N_2, and H_2/CO_2. The performance limit of polymer membranes is defined with the Robeson's upper bound[4,5] for different gas separations. The upper bound shows the single-component gas permeation data of polymers generally measured at 35 °C and 1–2 bar. Robeson upper bounds provide empirical relationships for membrane-based gas separation.[4,5] These upper bounds for several gas separations show the trade-off between membrane selectivity and gas permeability for polymeric membranes. The origin of the trade-off comes from the nature of glassy and rubbery polymers. Glassy polymers have restricted chain motions which yield low gas permeability, but they exhibit high membrane selectivity due to their strong size sieving ability.[95] On the other hand, rubbery polymers exhibit high gas permeability due to their high molecular chain mobility, but they provide low selectivity due to the ease of gas penetration through the flexible chains.[96] Since polymeric membranes have been commonly used for industrial applications, the performance of new membranes such as MOFs is assessed by considering these upper bounds. Due to a wide range of chemical environments and high porosities of MOFs, gas permeability and membrane selectivity of MOFs have been reported in a very large range.[97–99] In addition, when molecular sieving mechanism is used to assess the gas separation performances of MOF, extremely high membrane selectivities (up to 10^8) are reported in the literature.[72] For these reasons, it is difficult to observe a trade-off or define the upper-performance limits of MOF membranes. We used the experimental data of MOF membranes and MOF-based MMMs from a recent study[14] and collected the computational data from the corresponding studies listed in Table 1. The conditions for experimental and simulated permeation data that we collected from the literature are different in some cases and we direct the readers to the corresponding studies listed in Table 1.

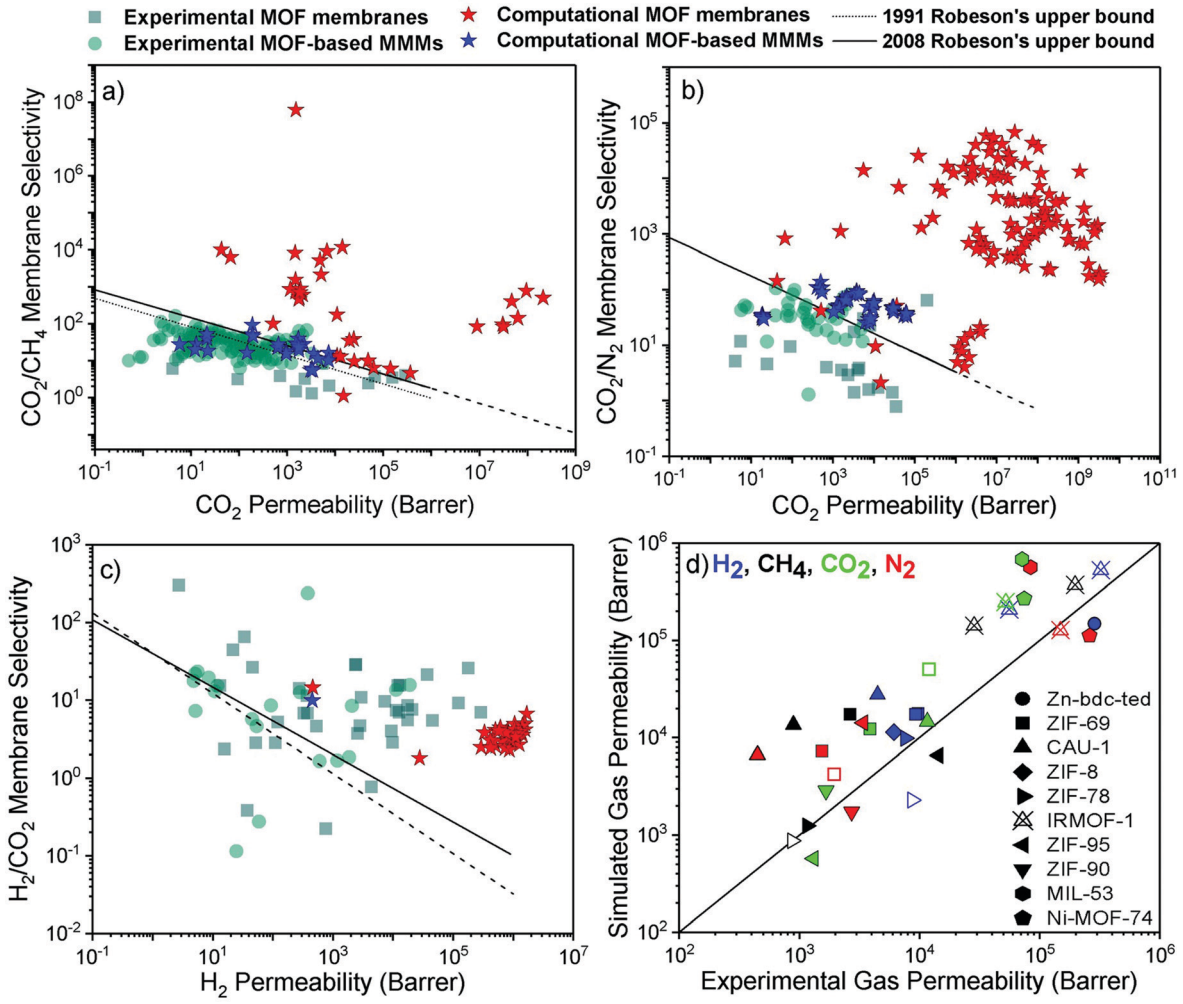

Fig. 3 Experimental and computational performance of MOF membranes and MOF-based MMMs for (a) CO_2/CH_4, (b) CO_2/N_2, and (c) H_2/CO_2 separations. The experimental data was redrawn based on the literature.[14] (d) Comparison of simulated and experimental gas permeabilities of 10 different MOFs. Filled (unfilled) symbols represent the single-component (mixture) gas permeability.

Table 1 Computational studies on MOF membranes and MOF-based MMMs

MOFs	Gas separation	Computational methodology	Simulation conditions	Performance metrics	Ref.
CAU-1	H_2/CH_4, CO_2/CH_4, CO_2/H_2, CO_2/N_2, Kr/Xe (SC, BM)	NEMD (dual-control plane (DCP))	1 bar, 298–600 K	Prm, S_{mem}	101
Cu-BTC	CH_4, C_2H_6, C_3H_8 (SC, BM, TM)	GCMC + EMD	4–55 bar, 298 K	D, S_{diff}, S_{mem}	117
ZIF-8	CH_4, C_2H_5, C_2H_6 (SC), C_2H_5/C_2H_6 (BM)	NEMD (Concentration gradient driven (CGD)-MD)	2–40 bar, 300 K	F, P, S_{mem}	84
Bio-MOF-11	CO_2/N_2 (BM)	GCMC + EMD	0–20 bar, 298 K	P, S_{diff}, S_{mem}	118
Cu-BDC	CO_2/CH_4 (BM)	NEMD	4.5–20 bar, 298 K	F, P, S_{mem}	119
ZIF-8	$H_2/N_2/CO_2$ (TM)	GCMC + EMD, NEMD (CGD-MD)	35 atm, 300 K	D, F, S_{mem}	65
ZIF-8, ZIF-67	C_3H_8, C_3H_7 (SC)	Maxwell–Stefan model	NA	D, S_{diff}	120
NH_2-MIL-53(Al)	CO_2 (SC)	GCMC + EMD	273 K	D	121
CAU-10-H MOF	CO_2, N_2, CH_4 (SC)	GCMC + EMD, TST	Infinite dilution, 300 K	Prm, P, S_{mem}	122
MOF-508a, MOF-508b	C_2H_2 (SC)	EMD	300–900 K	D	123
4 mixed-ligand MOFs	CH_4/H_2 (BM)	GCMC + EMD	0–20 bar, 298 K	P, S_{diff}, S_{mem}	124
MOF-5, CuBTC, ZIF-8, MEFMEQ	H_2/CH_4 (SC, BM)	GCMC + EMD, NEMD	1 bar, 2–4.5 bar, 298 K	F, P, S_{mem}	83
ZIF-8, ZIF-67	C_2H_6, C_2H_5 (SC)	EMD, TST	308 K	D, S_{diff}	125
ZIF-8, ZIF-7–8	CO_2, CH_4, N_2 (SC)	EMD, TST	Infinite dilution, 308 K	D, S_{diff}	71
ZIF-8, ZIF-67, BeIF-1, ZIF-7–8, Co-ZIF-7–8	He/CH_4, H_2/CH_4, O_2/N_2, CO_2/CH_4, CO_2/N_2 (SC)	TST	Infinite dilution, 308 K	P, S_{mem}	72
8 MOFs	CO_2, H_2, He, N_2, CH_4 (SC)	GCMC + EMD	~1 bar, ~298 K	Prm	56
8 MOFs	Xe/Kr, Xe/Ar (BM)	GCMC + EMD	0.1–25 bar, 298 K	P, S_{mem}	126
ZIF-8/PIM-1 MMM	H_2/CH_4 (SC, BM)	NEMD (CGD-MD)	5 bar, 300 K	P, S_{mem}	92
IL-modified ZIF-8/PI MMM	CO_2/CH_4 (SC)	GCMC + EMD	1–10 bar, 300 K	D, P, S_{diff}, S_{mem}	127
ZIF-7/PBI MMM	H_2/CO_2 (SC)	GCMC + EMD	Infinite dilution, 300 °C	D, P, S_{mem}	93
NUS-8/PIM-1 MMM	CO_2/N_2, CO_2/CH_4 (BM)	NEMD (CGD-MD)	10 bar, 298 K	P, S_{mem}	128
102 MOFs	N_2/CH_4 (BM)	GCMC + EMD	0.01 bar, 10 bar, 298 K	P, S_{diff}, S_{mem}	129
115 MOFs	Xe/Kr, Xe/Ar, Rn/Xe (BM)	GCMC + EMD	1 bar, 298 K	P, S_{mem}	130
172 MOFs	H_2/CH_4 (BM)	GCMC + EMD	10 bar, 298 K	P, S_{diff}, S_{mem}	102
175 MOFs	C_2H_6/C_2H_4, C_2H_6/CH_4 (BM)	GCMC + EMD	10 bar, 298 K	P, S_{diff}, S_{mem}	131
234 MOFs	H_2/CH_4 (SC)	GCMC + EMD	Infinite dilution, 300 K	D, P, S_{mem}	132
278 MOFs	C_2H_6/C_2H_4, C_2H_6/CH_4 (BM)	GCMC + EMD	10 bar, 298 K	D, P, S_{diff}, S_{mem}	46
288 COFs	H_2/CO_2 (BM)	GCMC + EMD	10 bar, 298 K	P, S_{mem}	133
298 COFs and 116 MMMs	CO_2/CH_4 (BM)	GCMC + EMD + MMM model	10 bar, 298 K	P, S_{mem}	134
500 MOFs	He/N_2 (SC)	GCMC + EMD	Infinite dilution, 298 K	S_{diff}, S_{mem}	135
504 MOFs + 165 Zeolites	H_2/CH_4 (SC)	GCMC + EMD	Infinite dilution, 298 K	P, S_{mem}	136
1163 MOFs	CO_2/N_2 (SC)	GCMC + EMD	Infinite dilution, 303 K	D, P, S_{diff}, S_{mem}	40
1525 MOFs	O_2/N_2 (BM)	GCMC + EMD	1 bar, 298 K	D, P, S_{diff}, S_{mem}	137
2932 MOFs	CO_2/CH_4 (BM)	GCMC + EMD	1 bar, 298 K	P, S_{diff}, S_{mem}	61
3080 MOFs	C_2H_4/C_2H_6 (SC)	TST	Infinite dilution, 298 K	D	73
3432 MOFs	Xe/Rn, Ar/Kr, Kr/Xe (SC)	GCMC + EMD, TST	Infinite dilution, 298 K	D, S_{diff}, S_{mem}	138
4764 MOFs	Hexane Isomers (SC, BM)	GCMC + EMD	Infinite dilution, 298 K, 10 bar, 433 K	P, S_{mem}	139
4764 MOFs	$CO_2/N_2/CH_4$ (TM)	GCMC + EMD	10 bar, 298 K	D, P, S_{diff}, S_{mem}	97
5600 MOFs	Xe/Kr (BM)	GCMC + EMD	1 bar, 298 K	D, S_{diff}, S_{mem}	140
6013 MOFs	CO_2, CH_4, O_2, N_2, H_2, H_2S, He (SC)	GCMC + EMD	Infinite dilution, 298 K	P, S_{mem}	141
12 020 MOF and 78 806 MMMs	O_2/N_2 (SC, BM, TM)	GCMC + EMD + MMM model	Infinite dilution, 1 bar, 298 K	P, S_{diff}, S_{mem}	142
54 808 MOFs	CO_2/H_2 (SC)	GCMC + EMD	Infinite dilution, 298 K	P, S_{diff}, S_{mem}	44
54 808 MOFs	CO_2/N_2 (SC, BM), $CO_2/N_2/H_2O$ (TM)	GCMC + EMD	Infinite dilution, 1 bar, 298 K	P, S_{diff}, S_{mem}	43
54 808 MOFs and 64 MMMs	CO_2/CH_4 (SC, BM)	GCMC + EMD + MMM model	Infinite dilution, 10 bar, 298 K	D, P, S_{diff}, S_{mem}	143
54 808 MOFs and 78 MMMs	H_2/N_2, $H_2/N_2/CO_2/CO$ (SC, BM, QM)	GCMC + EMD + MMM model	Infinite dilution, 1 bar, 298 K	P, S_{diff}, S_{mem}	144
67 675 MOFs	CO_2/CH_4, H_2S/CH_4 (SC, BM)	GCMC + EMD	Infinite dilution, 10 bar, 298 K	D, P, S_{mem}	145
70 551 MOFs	H_2/CO_2 (SC)	GCMC + EMD	Infinite dilution, 298 K	P, S_{diff}, S_{mem}	99
70 589 MOFs and 109 508 MMMs	CO_2/N_2 (SC, BM)	GCMC + EMD + MMM model	Infinite dilution, 1 bar, 298 K	P, S_{mem}	146
137 953 hMOFs	$CO_2/N_2/CH_4$ (SC, TM)	GCMC + EMD	Infinite dilution, 10 bar, 298 K	D, P, S_{diff}, S_{mem}	147
112 888 MOFs and 1 015 992 MMMs	CO_2/N_2 (SC)	GCMC + EMD + MMM model	Infinite dilution, 298 K	D, P, S_{diff}, S_{mem}	98

SC: single-component, BM: binary mixture, TM: ternary mixture, QM: quaternary mixture, P: permeability, F: flux, D: diffusivity, Prm: permeance.

Fig. 3(a) shows that although many MOF membranes and MOF-based MMMs, investigated either computationally or experimentally, exceed the Robeson's upper bound, there is still a trade-off between gas permeability and membrane selectivity for CO_2/CH_4 separation. While experimentally reported CO_2 permeabilities of MOF membranes are between 4–2.8 $\times$ 10^5 Barrers, selectivities are in the range of 1–13, indicating that experimentally measured MOF membranes are generally close to the upper bound. On the other hand, simulated CO_2/CH_4 selectivities and CO_2 permeabilities of MOF membranes are much higher than the experimental data which may be attributed to the high number and variety of MOFs considered in molecular simulations. Thin-film MOF membranes are frequently fabricated on a substrate and weak adhesion between MOF and the substrate may lead to nonselective openings for gas molecules. Defect formations and structural instability issues can also occur during fabrication of thin-film MOFs.[100] Because of these challenges in fabrication of thin-film MOF membranes, the variety of experimentally studied MOF-based MMMs is much more than that of thin-film MOF membranes. CO_2/CH_4 selectivities of MOF-based MMMs (9–164) are higher compared to those of pure MOF membranes but they still suffer from low permeability (0.5–5677 Barrers) to exceed the upper bound. We note that while the simulated performances of MOF membranes are well above the Robeson's upper bound due to the high gas permeability or high membrane selectivity, the simulated performance of MMMs is close to the upper bound because polymer phase dominates the performance of MMMs.

Fig. 3(b) shows that MOF membranes provide extremely high CO_2 permeability and CO_2/N_2 selectivity based on the results of molecular simulations. Here, we note that experimental gas permeance data for this separation is not currently available for many simulated MOFs; therefore, validation of the simulations is required to assess the actual performance of these membranes. Fig. 3(c) shows that simulated H_2/CO_2 selectivities are much lower compared to the experiments, although calculated H_2 permeabilities are much higher than the experimental H_2 permeabilities for many MOF membranes. The lighter and weakly adsorbed H_2 molecules diffuse faster through the pores than the strongly adsorbed CO_2 molecules, which enhances diffusion selectivity (S_{diff}) towards H_2. However, adsorption of CO_2 is much stronger than that of H_2 and CO_2 adsorption dominates the separation process. Therefore, calculated CO_2 permeabilities for many MOF membranes are much higher than H_2 permeabilities, leading to low membrane selectivity towards H_2. We note that structural flexibility is generally neglected in molecular simulations which also affects the separation performance of MOF membranes. To understand the accuracy of predicted gas separation performances of MOFs in Fig. 3(a)–(c), we compare simulated and experimental gas permeabilities of 10 different MOFs at the same conditions. We collected computational[43,56,101,102] and experimental studies[103–112] reporting single-component and mixture gas permeabilities of the same MOFs. Fig. 3(d) includes gas permeability data for 10 different MOF membranes (Zn-bdc-ted, ZIF-69, CAU-1, ZIF-78, ZIF-8, ZIF-90, ZIF-95, IRMOF-1, MIL-53 and Ni-MOF-74). In Fig. 3(d), different computational methodologies were used to simulate gas permeabilities of MOFs. For example, Adatoz and Keskin[56] used GCMC + EMD approach to compute H_2, N_2, CH_4 and CO_2 permeabilities of ZIF-69 and ZIF-8 and a good agreement was found between the theoretical and the experimental results of ZIF-8[113] and ZIF-69.[105] Zhai *et al.*[101] performed NEMD simulations to predict H_2, N_2, CH_4 and CO_2 permeabilities of CAU-1 and compared their predictions with experimental results reported by Yin *et al.*[112] Similarly to GCMC + EMD approach, NEMD method also agreed with experiments as shown in Fig. 3(d). However, simulated gas permeabilities generally overestimate experimental ones because MOFs are generally modelled as perfect, defect-free membrane materials which may not be true in experiments. Overall, Fig. 3(d) showed that although there can be generally deviations between predicted and experimental data of MOF membranes, the potentials of computational, not experimentally tested MOF-based membranes are shown. In the next section, we review some illustrative computational studies on MOF membranes.

3.1 Thin-film MOF membranes

We provided the information about computational studies on MOF-membranes and MOF-based MMMs in Table 1 by listing computational methodology, simulation conditions, and calculated membrane-based performance metrics. We provided the initial number of MOFs considered in high-throughput screening studies in Table 1. For example, Altintas *et al.*[46] firstly investigated the adsorption-based separation performances of 278 MOFs (we noted this number in Table 1) and then calculated membrane properties of only top 5 MOFs. Although thousands of MOFs have been synthesized and deposited into the CSD, the number of MOFs for which membrane properties are simulated and reported is very limited. Early computational works examined a very small number of MOFs. Table 1 demonstrates that ZIFs, especially ZIF-8, are widely studied due to their high potential in kinetic-driven gas separation, especially for gases having similar sizes with the pore sizes of ZIFs.[114] Due to their easy synthesizability and high chemical and thermal stabilities, available experimental data related to gas separation performances of ZIF membranes has rapidly increased.[115] This motivated computational researchers to focus on ZIF membranes. For example, GCMC + EMD simulations were performed to estimate the membrane properties of 8 different MOFs, including ZIF-8.[56] Predicted H_2 permeabilities of ZIF-8 at different conditions agreed well with the experimental measurements, showing that using this computational approach is reasonable and time-efficient to make accurate predictions about the properties of MOF membranes. Krokidas *et al.*[72] computationally investigated ZIF-8 and its tailored analogues based on the metal and/or linker replacement to assess their ideal He/CH_4, H_2/CH_4, O_2/N_2, CO_2/CH_4, and CO_2/N_2 separation performances. Instead of classical EMD simulations, they used TST[116] at infinite dilution to compute diffusivity coefficients. This study revealed that the systematic modification based on the replacement of building units of ZIF-8 can alter the performance of membranes by improving gas selectivity.

Table 1 shows that molecular simulations of MOF membranes are generally performed at single-component gas conditions. However, separation performance of MOF membranes for gas mixtures can be different at industrial operating conditions due to the competitive adsorption and diffusion between gas molecules. Therefore, mixture simulations which consider industrially relevant gas compositions are needed to unlock the real gas separation performances of MOF membranes. For example, Li *et al.*[118] predicted performance of Bio-MOF-11 membrane using GCMC + EMD approach for CO_2/N_2:15/85 and CO_2/N_2:50/50 mixture separations and showed that membrane selectivity of Bio-MOF-11 increases from $\sim$50 to $\sim$80 without a significant change in its CO_2 permeability (from 3.4×10^4 Barrer to 1.2×10^4 Barrer) when the mixture conditions are used in molecular simulations.

Based on the development in computational algorithms, high-throughput computational screening methodologies have gained a momentum in the MOF research. The advantage of screening studies is to identify the best membrane candidates from a very large number of MOFs. These studies produce a vast amount of data on MOFs which can be further used to establish structure-performance relations for the design and development of high-performance MOF membranes for a target gas separation. For example, 4240 MOFs in CSD MOF subset (over 10 000 in 2021) were screened by using GCMC + EMD approach and MOFs which have generally Cd, Cu, and Zn metals with narrow pores sizes (3.8–6 Å), low surface areas (<1000 m^2 g^{-1}), low porosities (<0.75) were found to be promising for H_2/CH_4 separation.[41] This kind of quantitative structure-performance relations are useful to choose the right membrane among the existing ones. In another study, 298 CoRE COFs (covalent organic framework), emerging class of crystalline networks consisted of covalently bonded light elements (H, C, N, O, B) with organic linkers,[148] were screened by GCMC + EMD simulations for membrane-based CO_2/CH_4 separation.[134] CO_2/CH_4 selectivities of COFs were found to be enhanced approximately 100 times by incorporating F^- and Cl^- groups into the framework compared to the selectivities of unmodified COFs. This result indicated that structural modifications can be a useful strategy to improve the separation performance of MOF and COF membranes to exceed the upper bound of polymers.

In addition to synthesized MOFs, computationally generated MOFs which are called hypothetical MOFs (hMOFs) were also screened to explore the structure-performance relationships. For example, Qiao *et al.*[147] used GCMC + EMD approach for 137 953 hMOFs[25] and showed that MOF membranes having narrow pore sizes ($\sim$3 Å) and large pore size distributions (PSD) in the range of 33–42% are the promising candidates for upgrading natural gas. They first performed simulations at infinite dilution and then for a small number of high-performing MOFs, simulations were repeated at practical operating conditions. This is a common strategy used in a multi-step screening approach to identify the promising MOF membranes. Recently, high-throughput screening approach was combined with the machine learning algorithms to predict performance metrics of 6103 CoRE MOFs with respect to six descriptors (pore limiting diameter (PLD), the largest cavity diameter (LCD), porosity, surface area, density, PSD) for different gas separations.[141] PLD was determined as the key parameter for predicting the membrane properties of MOFs especially for mixtures having more than three components. For the separation of binary gas mixtures, LCD and porosity were found to be more important. Using machine learning together with high-throughput computational screening can be effective to analyze the structure–property relations to guide the design of novel MOF membranes for a target gas separation.

In most of the computational studies, MOFs are assumed to be perfectly crystalline without any defects since accurate representation of the molecular interaction mechanism of gases on a defective surface is challenging. However, synthesized MOFs may have different types of intracrystalline defects which may affect their gas separation performance. To understand the effect of intracrystalline defects on H_2/CH_4 separation performances of MOF membranes, Kim *et al.*[132] used 234 DFT-minimized MOFs[149] and generated their defected structures with a Python script by randomly removing linkers. They used GCMC + EMD approach at infinite dilution to compute membrane properties. With the addition of linker vacancies, although many MOFs remained as promising, selectivities of the top performing MOFs significantly decreased as shown in Fig. 4(a) and (b). Therefore, it can be concluded that considering defects in molecular simulations can change our overall assessment about the top performing membranes. Thus, the selection of MOFs whose performances do not change when the linker vacancies are introduced will be a useful strategy to identify promising MOFs for industrial applications.

So far, we discussed GCMC + EMD approach which is based on the equilibrium conditions to predict membrane properties of MOF membranes. Velioglu and Keskin[83] compared calculated H_2 and CH_4 permeabilities and selectivities of ZIF-8 obtained from GCMC + EMD and NEMD simulations with the experiments in Fig. 5(a)–(c). Instead of using a fully flexible ZIF-8, they tethered the framework atoms during NEMD simulations and observed a faster gas diffusion compared to EMD.

Velioglu and Keskin[83] also provided the NEMD snapshots for pure and mixture gas permeations for H_2/CH_4 separation. In Fig. 5(d), they showed that CH_4 layer in the feed side is thick, referred to as concentration polarization at 1 ns whereas it reduces at 40 ns since at the starting point of the simulation an external force was applied. However, the concentration polarization was not observed for the binary mixture since H_2 accelerates the diffusion of slowly diffusing CH_4 (Fig. 5(e)). ZIF-8 was reported as a H_2 selective membrane in experiments (Fig. 5(c)). However, results obtained from GCMC + EMD simulations gave a higher CH_4 permeability, suggesting a CH_4 selective ZIF-8 membrane, compared to those obtained from NEMD. For this reason, NEMD simulations gave a better agreement with experiments as the range is represented with pattern-filled columns in Fig. 5(a)–(c) for both the single-component and mixture permeation of H_2 and CH_4 within ZIF-8 membrane. Thus, GCMC + EMD approach was suggested to quickly identify the most promising materials and then more

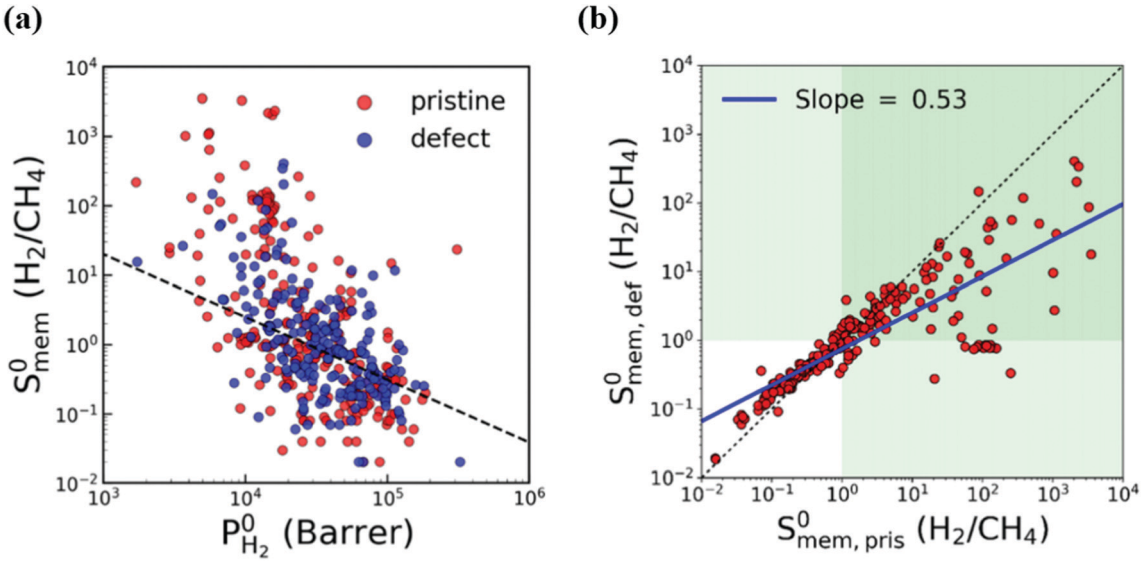

Fig. 4 Comparison of H_2/CH_4 membrane selectivity and H_2 permeability of pristine (red) and defective (blue) MOFs. The black dashed line represents the upper bound. The green area indicates H_2-selective region. The blue line is the least squares fit for the logarithm of the selectivities of pristine and defective structures. Reprinted from the study of Kim *et al.*[132]

detailed NEMD simulations which require longer simulation time (at least several days) are suggested to be used for the best membranes candidates to observe the mass transfer resistances on the pore entrance.

Namsani *et al.*[65] developed a new NEMD simulation method, concentration gradient driven molecular dynamics (CGD-MD),[84] to investigate H_2/N_2 and H_2/CO_2 separation performances of ZIF-8. Both GCMC + EMD and CGD-MD methods were applied by using four different force fields for ZIF-8. Regardless of the force field they used, ZIF-8 was identified as a H_2 selective membrane when the CGD-MD method was used whereas the membrane was found to be CO_2 selective when GCMC + EMD approach was used. Since the results of CGD-MD simulations agreed well with the experimental one,[150] this study reveals that at moderate or high-pressure conditions, a NEMD method such as CGD-MD is better to accurately predict the gas separation performance of MOF membranes.

All these studies show that accurate representation of the system and the operating conditions are important to model gas permeation through MOF membranes. In high-throughput screening studies, performing GCMC + EMD simulations is a practical approach to narrow down the materials space to point out the promising membranes due to the less computational power and time required compared to NEMD simulations. However, it should be kept in mind that GCMC + EMD simulations provide reliable results when gas molecules do not have a strong interaction with each other, especially at low pressures. On the other hand, mass transfer resistance on the membrane surface which affects the gas separation performance is not considered in this approach. For this reason, computationally costly NEMD simulations should be performed for the best performing membranes to ensure their potential for industrial applications. Here, if the MOF structure is flexible, considering the intramolecular forces is also important to figure out the realistic pore properties and performances of materials. We note that structural flexibility can be investigated by using GCMC + EMD or NEMD approaches. However, performing flexible simulations for screening applications is not convenient due to the enormous computational time and the difficulty to define intramolecular forces for each MOF structure. The effect of structural flexibility of MOFs on CO_2/CH_4 separation was investigated in our previous works.[143,151] Results showed that although membrane selectivity and permeability of a MOF having large pores slightly change when structural flexibility is considered, separation performances of MOFs having narrow pores close to the kinetic diameters of gases are dramatically affected. We finally conclude that both GCMC + EMD and NEMD approaches are useful to understand gas transport mechanisms in MOF membranes. However, researchers should be aware of the aforementioned limitations of these two approaches.

3.2 MOF-based MMMs

To overcome the trade-off between gas permeability and selectivity for polymeric membranes, MOFs are used as fillers in a polymeric matrix. Keskin and Sholl[152] used two theoretical permeation models, Maxwell[90] and Bruggeman,[87] to assess the separation performances of MOF-based MMMs. A good agreement between simulated and experimental permeation data of IRMOF-1/Matrimid was found indicating that theoretical models can give meaningful results for the performance prediction of MMM performances. Various gas permeation models such as Maxwell,[90] Modified Felske[153] were later used to compute the gas permeability of different types of MOF-based MMMs.[98,142]

Since the number of available MOFs and polymers is very high, using permeation models is practical in high-throughput computational screening to evaluate gas separation performances of a large number of MMMs. In some early studies, the best MOF membranes were initially selected *via* molecular simulations and properties of MMMs made of these MOFs were

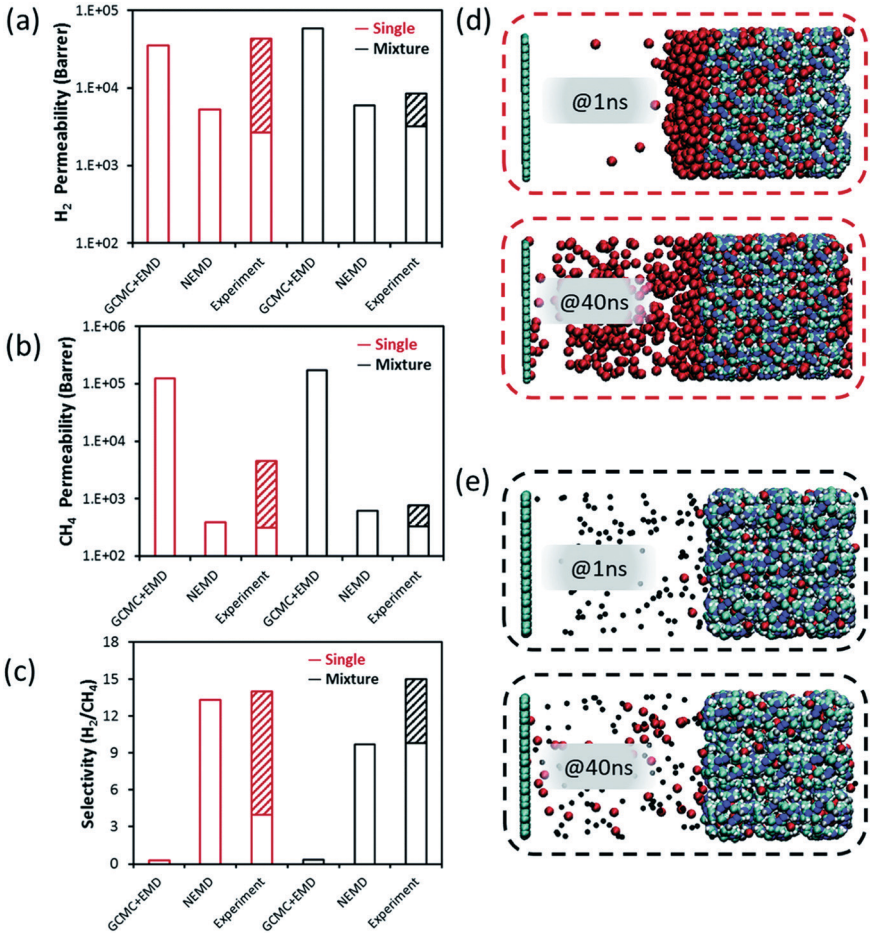

Fig. 5 Simulated (a) H_2 and (b) CH_4 permeabilities, (c) H_2/CH_4 membrane selectivity obtained from GCMC + EMD, NEMD simulations and their experimental values for ZIF-8. The hashed half-bars represent the range of experimental data reported in different studies. NEMD snapshots for permeation of (d) pure CH_4, (e) H_2/CH_4 mixture at the 1st and 40th ns. The dark blue, white, cyan, and colors represent zinc, hydrogen, and carbon atoms, respectively in (d and e). Black (red) colors also represent H_2 (CH_4) molecules, respectively in (d and e). Reprinted from the study of Velioglu and Keskin.[83]

then predicted using permeation models.[143,144] Another way is to compute gas permeability of a large number of MMMs considering many MOF/polymer combinations and then identify the best ones offering the desired MMM properties.[146] It is important to note that the properties of MOF and polymer have a synergetic effect on those of MMMs. In our previous studies,[142–144,146] we showed that when a MOF filler is incorporated into a low permeable polymer, it generally affects gas permeability without any change in membrane selectivity. On the other hand, when the same MOF is incorporated into a highly permeable polymer, it can probably change both gas permeability and membrane selectivity of the polymer since the identity of MOF filler gains importance for highly permeable (>1000 Barrer) polymers. Therefore, a careful selection of MOF and polymer pairs for high performing MMMs is very important. We note that these approaches assume perfect compatibility between MOF/polymer interface. Gas separation performance of polymer dominates the predicted separation properties of MOF-based MMMs which is called percolation threshold.[154] The reason is that rubbery polymers having flexible chains are commonly used to make defect-free and compatible MMMs, but these flexible chains lead to highly permeable regions for gas molecules. This was clearly represented in the literature[98] in which properties of CoRE MOF-based MMMs were predicted *via* atomistic and continuum approach at infinite dilution for CO_2/N_2 separation. In Fig. 6(a), while square symbol represents the CO_2 permeability of pure polymers, the line represents the relationship between CO_2 permeability of MMMs and the ratio of permeability of MOF and polymer. This figure gives an important message to understand the effect of the MOF-polymer relation on the separation performances of MMMs. Fig. 6(a) showed that when MOF filler exhibits lower gas permeability than the related polymer, the gas permeability of the MMM consisting of this MOF-polymer pair is lower than pure polymer and *vice versa*. On the other hand, if gas permeability of MOF is higher than that of polymer, it may enhance the permeability of polymer. Perhaps the most critical result is that if gas permeability of a MOF is at least 10 times higher than that of the polymer, polymer performance cannot be further improved. Therefore, even if gas permeability of a MOF is extremely higher than that of polymer, the maximum achievable gas permeabilities of MMMs is ~2 times

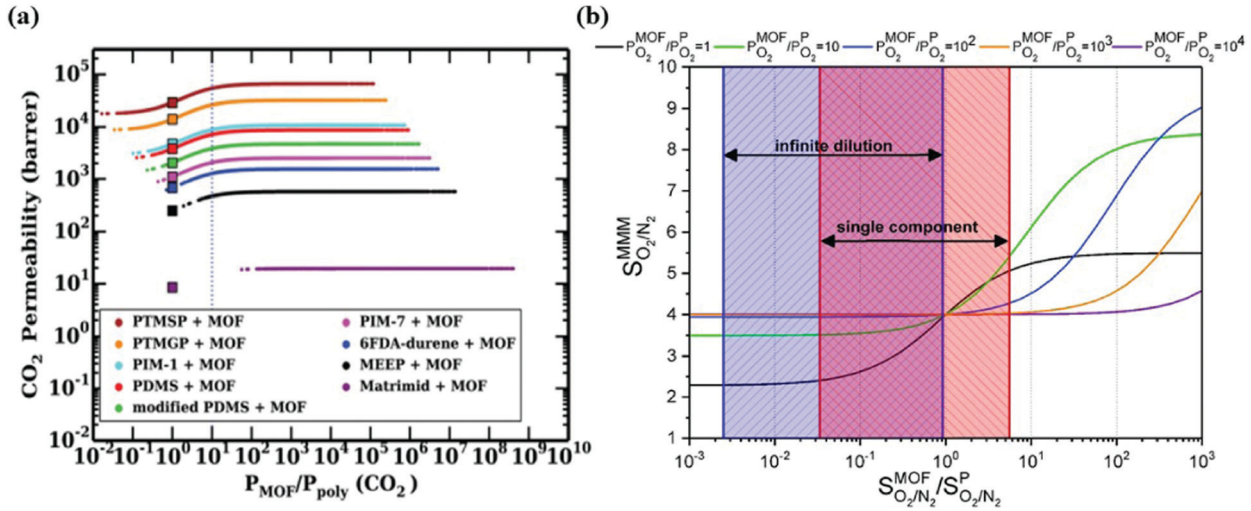

Fig. 6 (a) Relations between CO_2/N_2 selectivity of MMMs, MOFs, and polymers. Square symbols show CO_2 permeabilities of pure polymers. Reprinted from the study of Budhathoki *et al.*[98] (b) O_2/N_2 selectivity of MMMs as a function of the ratio of the selectivity of MOF over the selectivity of polymer (PIM-1 with a selectivity of 4). Reprinted from the study of Daglar *et al.*[142]

the permeability of related polymers based on Maxwell model.[98,143]

Similar results were also observed in our recent work[142] where O_2 permeability and O_2/N_2 selectivity of 78 806 MMMs composed of 5629 MOFs and 14 different polymers were estimated by using the Maxwell model. The effect of membrane selectivity of MOFs and polymer (PIM-1 as a reference polymer) on the overall selectivity of MMMs was examined as a function of the ratio of gas permeability of MOFs and polymer. As shown in Fig. 6(b), if selectivity of MOF is lower than selectivity of polymer, it is not possible to obtain a MMM selectivity higher than that of polymer regardless of the gas permeability ratio. In other words, improving the O_2/N_2 selectivity of polymer is only possible by using MOFs having higher selectivity compared to polymer. In high-throughput screening studies on MMMs, although polymer permeability data used in theoretical models is generally measured at single-component gas conditions, simulations of MOFs are performed at infinite dilution to reduce the computational cost.[98,146] We also showed that when molecular simulations of MOFs are performed at infinite dilution (considering only one gas molecule in the framework), the results underestimated O_2/N_2 membrane selectivities of MMMs calculated at single-component gas conditions (1 bar, 298 K). This result can be explained by the existence of gas-gas interactions at 1 bar and showed that simulation conditions of MOFs affect the predicted performance of MMMs. Therefore, using the same simulation conditions with experimental ones is critical to unlock the potential of MMMs.

Although gas permeation models are useful to predict gas permeabilities and selectivities of MOF/polymer MMMs, they do not consider the size and morphology of MOFs and the interfacial compatibility between polymer and MOF phases. We noted that MOF-polymer compatibility can be different based on the selection of MOF-polymer pairs, and it depends on not only the properties of MOF such as crystalline size and shape but also the properties of polymer such as rigidity. Therefore, fully atomistic simulations which consider models for both MOF and polymer phases are necessary. The first example of a fully atomistic simulation for MOF/polymer MMMs was reported for ZIF-7/PBI for H_2/CO_2 separation.[93] ZIF-7/PBI MMM model membranes were constructed considering different ZIF-7 cages and sorption and diffusion properties of H_2 and CO_2 were predicted using GCMC + EMD approach at 300 °C and infinite dilution. The relationship between gas transport mechanism and gas density distributions in 1-cage ZIF-7/PBI membrane revealed that CO_2 cannot diffuse through the small interfacial voids at the interface between ZIF-7 and PBI in contrast to H_2 molecules which locate at both ZIF-7 cages and PBI. Therefore, CO_2 diffusion decreased with the increase in the number of ZIF-7 cages. Overall, results showed that permeability of H_2 and CO_2 in ZIF-7/PBI MMM is enhanced with the increase in ZIF-7 loading compared to those in pure PBI whereas H_2/CO_2 selectivities do not significantly change. Although these results are encouraging, a critical part which is the modelling of the interfacial morphology between MOF and polymer phases was missing.

To fabricate a high-performance MOF-based MMM, the proper selection of MOF and polymer pairs is important because the interfacial compatibility between those is generally poor and agglomeration which diminishes the gas separation performance of membranes may occur.[154,155] Recently, Dutta *et al.*[127] examined the interfacial characteristics of ZIF-8/6FDA-durane polyimide MMMs for CO_2/CH_4 separation using GCMC + EMD approach. To enhance the compatibility of the interface between ZIF-8 and polymer, they used an IL (ionic liquid), which filled the larger voids in the interface between ZIF-8 and 6FDA-durane polyimide polymer. With the incorporation of IL, CO_2/CH_4 membrane selectivity of MMM increased without a significant change in its permeability and this MMM surpassed the upper bound. Maurin's group[94] developed an interface model to

understand the compatibility between ZIF-8 and PIM-1 (polymer of intrinsic microporosity-1). The compatibility at ZIF-8/PIM-1 interface was shown with the interactions between CN groups of PIM-1 and NH groups of ZIF-8. This model was also applied to different MOF/polymer systems such as UiO-66/6FDA-DAM[156] and HKUST-1/poly(vinyl alcohol).[157] In the further study of this group,[92] they showed that if atomistic and continuum modelling are used to predict ideal H_2/CH_4 membrane selectivities of ZIF-8/PIM-1 MMMs, higher selectivities are obtained compared to those obtained from CGD-MD simulations. Ozcan *et al.*[92] showed that H_2/CH_4 selectivity of ZIF-8/PIM-1 MMM is lower (4.6) than the selectivity of the pure ZIF-8 (5.1) and PIM-1 (6.3) due to non-selective regions occurred at the interface. This result again supports the idea that properties of MOF and polymer have a synergetic effect on the property of MMMs. On the other hand, when CGD-MD were performed for equimolar H_2/CH_4 mixture for PIM-1/ZIF-8 MMMs, lower H_2/CH_4 selectivities were found than those computed at single-component gas condition. Overall, simulation conditions affect the gas separation performances of MOF-based MMMs and accurate definition of these conditions in molecular simulations is important. We also noted that there is a common idea in the literature that interfacial porosity has a negative effect on the gas separation performances of MMMs. However, Fan *et al.*[128] very recently showed that the porosity at the interface of NUS-8/PIM-1 MMM leads to an increase in membrane selectivity for MMMs due to the enhanced CO_2-MOF interactions.

3.3 Comparison of simulated and experimental performances of MOF membranes

Molecular simulations are highly useful to provide insights into the gas permeation through MOF-based MMMs. To show the validity of computational methodologies for predicting gas permeation through membranes, comparing simulation results with experimental measurements for various gas separations is required. For validation, molecular simulations are computed at the same pressure and temperature with the experiments and then compared with the experiments in several studies.[43,144] For example, Wilmer *et al.*[98] calculated CO_2 and N_2 permeabilities of 11 different MOF-based MMMs using Maxwell Model and compared their predictions with experimental measurements as shown in Fig. 7(a). The good agreement between predicted and experimental gas permeabilities validated their computational methodology. Similarly, our group compared experimental and simulated CO_2 and N_2 permeabilities of 13 MOF-based MMMs composed of 6 different MOFs and 7 different polymers at the same conditions with experiments.[146] We showed that although simulation results agree well with experiments, they generally underestimate experiments as the weight percentage of MOF in polymer increases. In molecular simulations, we generally assume that MOFs are defect-free crystals and MOF/polymer pairs are perfectly compatible to generate MMMs. However, experimentally fabricated MMMs may have defects which can enhance gas diffusion through membranes. In addition, an increase of MOF loading in the polymer may cause agglomeration in MMM, which may play a critical role in creating non-selective regions for gas transport. In computational studies, theoretical permeation models such as Modified Felske and Maxwell are generally used to predict gas permeabilities of MMMs and these models do not consider particle interactions, an important issue especially at high filler loadings. Therefore, these models are noted to be applicable to the MMMs for which low loadings (filler volume fraction range < 0.2) of MOF filler are incorporated into the polymer.[158] For these reasons, a much higher gas permeability can be reported by the experiments compared to simulations.

On the other hand, direct comparisons of simulation results with experiments are not available in some studies due to the lack of available experimental data in the literature. For example, as we discussed before ZIF-7/PBI MMM was constructed to investigate its H_2/CO_2 separation performance.[93] In Fig. 7(b), to validate the accuracy of their predictions, it is required to

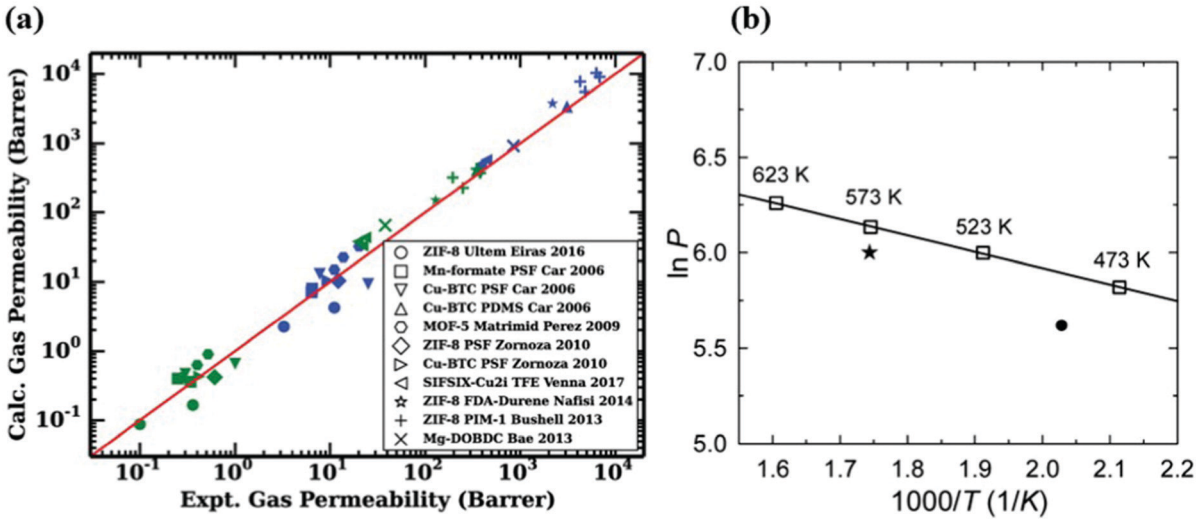

Fig. 7 (a) Comparison of experimental and simulated CO_2 (blue) and N_2 (green) permeabilities of 11 different MMMs. Reprinted from the study of Budhathoki *et al.*[98] (b) The relationship between H_2 permeability of ZIF-7 and temperature. The line is the Arrhenius fit based on the simulation data (squares). The circle is the available experimental data at 220 °C and the star is extrapolated at 300 °C. Reprinted from the study of Zhang *et al.*[93]

compare the simulated H_2 permeability with experimental data at the same conditions. Since there is no available H_2 permeability data of ZIF-7 at 573 K, Zhang *et al.*[93] first fitted simulated data at various temperatures by using Arrhenius equation. Then, they used the Arrhenius fit line to extrapolate available experimental data at 493 K to the data at 573 K. Although predicted H_2 and CO_2 permeabilities were 461 and 32 Barrers, extrapolated gas permeabilities were reported as 408 and 22 Barrers, respectively, resulting in a fairly good agreement between experimental and simulated permeabilities. We noted that the change in temperature can affect the gas permeability and membrane selectivity. As temperature increases, the amount of adsorbed gas molecules decreases whereas the diffusivity of adsorbed molecules increases. Since gas permeability is the combination of adsorption and diffusion properties of MOFs, it also changes with temperature. The relationship between gas permeability and temperature can be also described by Arrhenius equation, ($P \propto \exp(-E_a/RT)$) where E_a is the activation energy (J mol^{-1}), R is the ideal gas constant (J K^{-1} mol^{-1}), and T is the temperature (K). Several studies also showed that, gas permeability generally increases as temperature increases based on Arrhenius equation.[93,159–161] In addition, although an inverse relationship between membrane selectivity and temperature can be observed in the literature,[160] the effect of temperature on membrane selectivity depends on the type of gas separation applications. Overall, the validation step is critical for assessing the reliability of computational methodologies and molecular simulations should be performed under the same conditions with the experiments to make a direct comparison.

4. Outlook

In this study, we reviewed the current state-of-the-art computational methods to predict gas permeation through MOF membranes and MOF-based MMMs. We finally address the following topics to be considered in future studies:

• As we discussed throughout this review, the membrane performances of pristine MOF membranes and MOF-based MMMs can be predicted by different computational methodologies such as GCMC + EMD and NEMD. Perhaps, the most important step to prove the reliability of these methods is to compare simulation results with the experimental data. However, due to the lack of available experimental data on a variety of MOFs, this crucial step is missing in many studies. Therefore, the results obtained from simulations should be compared at least with the available experimental measurements before providing all simulated data of different types of MOF membranes.

• The number of MOFs for which membrane properties are simulated and reported is very limited because EMD and NEMD simulations require higher computational time (up to hundreds of CPU hours per material) compared to GCMC simulations. Since computing diffusion properties of MOFs are computationally demanding, more practical ways for predicting diffusion coefficients are needed to increase the number of studies on MOF membranes. Recently, Wu and Zhou[73] developed a massively parallel graphic processing unit (GPU)-accelerated string method by using TST to calculate the diffusivity for MOFs. They showed that by using this method, diffusion calculations can be completed significantly faster (<30 seconds) than conventional MD simulations.

• Currently, all computational studies identify the best MOF membranes or MOF-based MMMs based on the ability of membranes to surpass the Robeson's upper bound. Since Robeson's upper bound is defined for single-component gas permeation, the upper limits of gas separation performances of polymers can be different for mixtures, thus it should be a reference line rather than a standard line for gas mixtures. In addition, separation performance of real MOF membranes can be also significantly different when gas mixtures at industrial conditions are considered. Therefore, performing computational studies considering gas mixtures at different operation conditions is necessary to get a more realistic predictions for the membranes.

• The thickness of the thin-film MOF membrane directly affects the measured gas flux and selectivity. For example, synthesis of one of the thinnest ZIF-8 membranes, 300–400 nm, revealed that this ZIF-8 gives one of the highest propylene/propane selectivity (120) among other reported ZIF-8 membranes in the literature.[162] In NEMD simulations, the thickness is defined in the range of 40–50 Å to save computational time and sources.[81,163] However, the thickness of fabricated MOF membranes is generally much larger (>25 μm). Membrane thickness considered in simulations can also affect gas separation performances of membranes. For example, Wang *et al.*[164] performed NEMD simulations to understand the effect of carbon membrane thickness on gas flux for O_2/N_2 separation. Their results showed that as the membrane thickness increases, both O_2 and N_2 fluxes decrease due to the increase in membrane resistance. Overall, using larger membrane thickness when calculating gas flux in NEMD simulations can be important.

• In molecular simulations, defect-free, purely crystalline and rigid MOF structures are generally assumed. Considering structural stability in molecular simulations is not a trivial task since it requires DFT calculations. However, at least for the promising membrane candidates, DFT calculations can be performed to ensure the structural stability of membrane material. In addition, predictions for mechanical properties of MOF membranes such as Young's modules and mechanical strength will also be highly useful to guide experimental studies. Coudert and coworkers performed molecular simulations to understand the mechanical properties of MIL-53,[165] UiO-66,[166,167] and ZIF-8.[168] Moghadam *et al.*[169] performed a multi-level computational analysis to predict mechanical stability of MOFs and investigated the relationship between structural properties (*i.e.*, topology) and mechanical strength (bulk modulus) of 3385 hypothetical MOFs. Examining experimentally synthesized MOF subsets would be also interesting. In addition, the mechanical strength of MOFs should be also investigated during gas separation process, which is currently missing in the literature.

• In high-throughput computational screening studies on MOF-based MMMs,[98,143,146] molecular simulations for MOFs

are generally performed at infinite dilution or at 1 bar, 298 K regardless of the measurement conditions of polymers. However, combining the performance data of a polymer tested at a different pressure range (up to 10 bar)[170–176] with the performance data of MOFs predicted at infinite dilution may lead to unrealistic gas separation performance for MOF-polymer pairs. Therefore, simulation conditions for MOFs should be the same with the experimental conditions of polymers.

- The ultimate aim of high-throughput computational screening is to identify the top MOF membranes considering their ranking based on gas permeability and/or selectivity. However, the top membranes identified from high-throughput computational screening studies should be experimentally tested. Collaborative studies in which both experimentalists and theoreticians including engineers, chemists, materials scientists work together will be extremely useful for the design, development and testing of new MOF membranes.

Conflicts of interest

There are no conflicts to declare.

Acknowledgements

S. K. acknowledges ERC-2017-Starting Grant. This study has received funding from the European Research Council (ERC) under the European Union's Horizon 2020 research and innovation programme (ERC-2017-Starting Grant, grant agreement No 756489-COSMOS).

References

1 Y. Ding, *Ind. Eng. Chem. Res.*, 2020, **59**, 556–568.
2 Q. Qian, P. A. Asinger, M. J. Lee, G. Han, K. Mizrahi Rodriguez, S. Lin, F. M. Benedetti, A. X. Wu, W. S. Chi and Z. P. Smith, *Chem. Rev.*, 2020, **120**, 8161–8266.
3 J. Yu, L.-H. Xie, J.-R. Li, Y. Ma, J. M. Seminario and P. B. Balbuena, *Chem. Rev.*, 2017, **117**, 9674–9754.
4 L. M. Robeson, *J. Membr. Sci.*, 1991, **62**, 165–185.
5 L. M. Robeson, *J. Membr. Sci.*, 2008, **320**, 390–400.
6 O. M. Yaghi, M. O'Keeffe, N. W. Ockwig, H. K. Chae, M. Eddaoudi and J. Kim, *Nature*, 2003, **423**, 705–714.
7 Q. Yang, Q. Xu and H.-L. Jiang, *Chem. Soc. Rev.*, 2017, **46**, 4774–4808.
8 Y. Cui, Y. Yue, G. Qian and B. Chen, *Chem. Rev.*, 2012, **112**, 1126–1162.
9 Z. Hu, B. J. Deibert and J. Li, *Chem. Soc. Rev.*, 2014, **43**, 5815–5840.
10 M. Eddaoudi, J. Kim, N. Rosi, D. Vodak, J. Wachter, M. O'Keeffe and O. M. Yaghi, *Science*, 2002, **295**, 469–472.
11 X. Li, Y. Liu, J. Wang, J. Gascon, J. Li and B. Van der Bruggen, *Chem. Soc. Rev.*, 2017, **46**, 7124–7144.
12 K. Adil, Y. Belmabkhout, R. S. Pillai, A. Cadiau, P. M. Bhatt, A. H. Assen, G. Maurin and M. Eddaoudi, *Chem. Soc. Rev.*, 2017, **46**, 3402–3430.
13 M. R. A. Hamid and H.-K. Jeong, *Korean J. Chem. Eng.*, 2018, **35**, 1577–1600.
14 N. Prasetya, N. F. Himma, P. D. Sutrisna, I. G. Wenten and B. P. Ladewig, *Chem. Eng. J.*, 2019, 123575.
15 E. Adatoz, A. K. Avci and S. Keskin, *Sep. Purif. Technol.*, 2015, **152**, 207–237.
16 J. Yao and H. Wang, *Chem. Soc. Rev.*, 2014, **43**, 4470–4493.
17 B. Seoane, J. Coronas, I. Gascon, M. E. Benavides, O. Karvan, J. Caro, F. Kapteijn and J. Gascon, *Chem. Soc. Rev.*, 2015, **44**, 2421–2454.
18 M. S. Denny, J. C. Moreton, L. Benz and S. M. Cohen, *Nat. Rev. Mater.*, 2016, **1**, 1–17.
19 Y. Zhang, X. Feng, S. Yuan, J. Zhou and B. Wang, *Inorg. Chem. Front.*, 2016, **3**, 896–909.
20 F. H. Allen, *Acta Crystallogr., Sect. B: Struct. Sci.*, 2002, **58**, 380–388.
21 H. Daglar and S. Keskin, *Coord. Chem. Rev.*, 2020, **422**, 213470.
22 D. Ongari, L. Talirz and B. Smit, *ACS Cent. Sci.*, 2020, **6**, 1890–1900.
23 P. Z. Moghadam, A. Li, S. B. Wiggin, A. Tao, A. G. Maloney, P. A. Wood, S. C. Ward and D. Fairen-Jimenez, *Chem. Mater.*, 2017, **29**, 2618–2625.
24 Y. G. Chung, E. Haldoupis, B. J. Bucior, M. Haranczyk, S. Lee, H. Zhang, K. D. Vogiatzis, M. Milisavljevic, S. Ling and J. S. Camp, *J. Chem. Eng. Data*, 2019, **64**, 5985–5998.
25 C. E. Wilmer, M. Leaf, C. Y. Lee, O. K. Farha, B. G. Hauser, J. T. Hupp and R. Q. Snurr, *Nat. Chem.*, 2012, **4**, 83.
26 M. J. C. Ordonez, K. J. Balkus Jr, J. P. Ferraris and I. H. Musselman, *J. Membr. Sci.*, 2010, **361**, 28–37.
27 A. Huang, H. Bux, F. Steinbach and J. Caro, *Angew. Chem., Int. Ed.*, 2010, **49**, 4958–4961.
28 F. M. Benedetti, M. G. De Angelis, M. Degli Esposti, P. Fabbri, A. Masili, A. Orsini and A. Pettinau, *Membranes*, 2020, **10**, 56.
29 G. Avci, S. Velioglu and S. Keskin, *ACS Appl. Mater. Interfaces*, 2018, **10**, 33693–33706.
30 P. M. Morse, *Phys. Rev.*, 1929, **34**, 57.
31 G. Von Mie, *Ann. Phys.*, 1903, **11**, 657–697.
32 R. A. Buckingham, *The classical equation of state of gaseous helium, neon and argon*, 1938, vol. 168, pp. 264–283.
33 J. E. Lennard-Jones, *Proc. Phys. Soc.*, 1931, **43**, 461.
34 D. Halliday, R. Resnick and J. Walker, *Fundamentals of physics*, John Wiley & Sons, 2013.
35 A. K. Rappé, C. J. Casewit, K. Colwell, W. Goddard Iii and W. Skiff, *J. Am. Chem. Soc.*, 1992, **114**, 10024–10035.
36 S. L. Mayo, B. D. Olafson and W. A. Goddard, *J. Phys. Chem.*, 1990, **94**, 8897–8909.
37 S. Bureekaew, S. Amirjalayer, M. Tafipolsky, C. Spickermann, T. K. Roy and R. Schmid, *Phys. Status Solidi B*, 2013, **250**, 1128–1141.
38 J. K. Bristow, D. Tiana and A. Walsh, *J. Chem. Theory Comput.*, 2014, **10**, 4644–4652.
39 J. G. McDaniel, S. Li, E. Tylianakis, R. Q. Snurr and J. Schmidt, *J. Phys. Chem. C*, 2015, **119**, 3143–3152.
40 T. Watanabe and D. S. Sholl, *Langmuir*, 2012, **28**, 14114–14128.

41 C. Altintas, G. Avci, H. Daglar, E. Gulcay, I. Erucar and S. Keskin, *J. Mater. Chem. A*, 2018, **6**, 5836–5847.
42 C. Altintas, G. Avci, H. Daglar, A. Nemati Vesali Azar, S. Velioglu, I. Erucar and S. Keskin, *ACS Appl. Mater. Interfaces*, 2018, **10**, 17257–17268.
43 H. Daglar and S. Keskin, *J. Phys. Chem. C*, 2018, **122**, 17347–17357.
44 G. Avci, S. Velioglu and S. Keskin, *ACS Appl. Mater. Interfaces*, 2018, **10**, 33693–33706.
45 O. Kadioglu and S. Keskin, *Sep. Purif. Technol.*, 2018, **191**, 192–199.
46 C. Altintas and S. Keskin, *Chem. Eng. Sci.*, 2016, **139**, 49–60.
47 J. J. Potoff and J. I. Siepmann, *AIChE J.*, 2001, **47**, 1676–1682.
48 Y. Sun, D. Spellmeyer, D. A. Pearlman and P. Kollman, *J. Am. Chem. Soc.*, 1992, **114**, 6798–6801.
49 D. D. Do and H. D. Do, *J. Phys. Chem. B*, 2005, **109**, 19288–19295.
50 V. Buch, *J. Chem. Phys.*, 1994, **100**, 7610–7629.
51 Q. Yang and C. Zhong, *J. Phys. Chem. B*, 2005, **109**, 11862–11864.
52 Q. Yang and C. Zhong, *J. Phys. Chem. B*, 2006, **110**, 655–658.
53 J. G. Harris and K. H. Yung, *J. Phys. Chem.*, 1995, **99**, 12021–12024.
54 C. Mellot and J. Lignieres, *Mol. Simul.*, 1997, **18**, 349–365.
55 K. Makrodimitris, G. K. Papadopoulos and D. N. Theodorou, *J. Phys. Chem. B*, 2001, **105**, 777–788.
56 E. Adatoz and S. Keskin, *J. Nanomater.*, 2015, **2015**, 1–9.
57 C. E. Wilmer and R. Q. Snurr, *Chem. Eng. J.*, 2011, **171**, 775–781.
58 T. A. Manz and D. S. Sholl, *J. Chem. Theory Comput.*, 2010, **6**, 2455–2468.
59 C. M. Breneman and K. B. Wiberg, *J. Comput. Chem.*, 1990, **11**, 361–373.
60 C. Campañá, B. Mussard and T. K. Woo, *J. Chem. Theory Comput.*, 2009, **5**, 2866–2878.
61 C. Altintas and S. Keskin, *Mol. Syst. Des. Eng.*, 2020, **5**, 532–543.
62 R. W. Baker and B. T. Low, *Macromolecules*, 2014, **47**, 6999–7013.
63 J. G. Wijmans and R. W. Baker, *J. Membr. Sci.*, 1995, **107**, 1–21.
64 D. Frenkel and B. Smit, *Understanding molecular simulation: From algorithms to applications*, Elsevier (formerly published by Academic Press), 2002, vol. 1, pp. 1–638.
65 S. Namsani, A. Ozcan and A. Ö. Yazaydın, *Adv. Theory Simul.*, 2019, **2**, 1900120.
66 P. P. Ewald, *Ann. Phys.*, 1921, **369**, 253–287.
67 A. I. Skoulidas and D. S. Sholl, *J. Phys. Chem. B*, 2005, **109**, 15760–15768.
68 A. H. Farmahini, S. Krishnamurthy, D. Friedrich, S. Brandani and L. Sarkisov, 2020, arXiv preprint arXiv:2009.12289.
69 J. Kärger and D. M. Ruthven, *New J. Chem.*, 2016, **40**, 4027–4048.
70 R. L. June, A. T. Bell and D. N. Theodorou, *J. Phys. Chem.*, 1991, **95**, 8866–8878.
71 P. Krokidas, S. Moncho, E. N. Brothers, M. Castier, H.-K. Jeong and I. G. Economou, *ACS Appl. Mater. Interfaces*, 2018, **10**, 39631–39644.
72 P. Krokidas, S. Moncho, E. N. Brothers and I. G. Economou, *ACS Appl. Mater. Interfaces*, 2020, **12**, 20536–20547.
73 M. Zhou and J. Wu, *ACS Appl. Nano Mater.*, 2021, **4**, 5394–5403.
74 B. Widom, *J. Chem. Phys.*, 1963, **39**, 2808–2812.
75 D. Dubbeldam, E. Beerdsen, T. Vlugt and B. Smit, *J. Chem. Phys.*, 2005, **122**, 224712.
76 G. Arya, H.-C. Chang and E. J. Maginn, *J. Chem. Phys.*, 2001, **115**, 8112–8124.
77 D. A. Newsome and D. S. Sholl, *J. Phys. Chem. B*, 2005, **109**, 7237–7244.
78 H. Babaei, A. J. McGaughey and C. E. Wilmer, *ACS Appl. Mater. Interfaces*, 2018, **10**, 2400–2406.
79 M. Fasano, T. Humplik, A. Bevilacqua, M. Tsapatsis, E. Chiavazzo, E. N. Wang and P. Asinari, *Nat. Commun.*, 2016, **7**, 12762.
80 M. J. Berry, C. M. Taylor, W. King, Y.-M. Chew and J. Wenk, *Water*, 2017, **9**, 452.
81 K. N. Han, S. Bernardi, L. Wang and D. J. Searles, *J. Membr. Sci.*, 2015, **495**, 322–333.
82 T. Kovács, S. Papp and T. Kristóf, 2017, arXiv preprint arXiv:1706.07250.
83 S. Velioglu and S. Keskin, *J. Mater. Chem. A*, 2019, **7**, 2301–2314.
84 A. Ozcan, C. Perego, M. Salvalaglio, M. Parrinello and O. Yazaydin, *Chem. Sci.*, 2017, **8**, 3858–3865.
85 G. S. Heffelfinger and F. v. Swol, *J. Chem. Phys.*, 1994, **100**, 7548–7552.
86 K. M. Gupta, Z. Qiao, K. Zhang and J. Jiang, *ACS Appl. Mater. Interfaces*, 2016, **8**, 13392–13399.
87 G. Banhegyi, *Colloid Polym. Sci.*, 1986, **264**, 1030–1050.
88 R. Pal, *J. Reinf. Plast. Compos.*, 2007, **26**, 643–651.
89 J. Felske, *Int. J. Heat Mass Transf.*, 2004, **47**, 3453–3461.
90 J. Maxwell, *Electricity and magnetism*, Dover, New York, 1954, vol. 2.
91 I. Erucar and S. Keskin, *Ind. Eng. Chem. Res.*, 2011, **50**, 12606–12616.
92 A. Ozcan, R. Semino, G. Maurin and A. O. Yazaydin, *Chem. Mater.*, 2020, **32**, 1288–1296.
93 L. Zhang, Z. Hu and J. Jiang, *J. Phys. Chem. C*, 2012, **116**, 19268–19277.
94 R. Semino, N. A. Ramsahye, A. Ghoufi and G. Maurin, *ACS Appl. Mater. Interfaces*, 2016, **8**, 809–819.
95 L. M. Robeson, Z. P. Smith, B. D. Freeman and D. R. Paul, *J. Membr. Sci.*, 2014, **453**, 71–83.
96 L. M. Robeson, Q. Liu, B. D. Freeman and D. R. Paul, *J. Membr. Sci.*, 2015, **476**, 421–431.
97 Z. Qiao, Q. Xu and J. Jiang, *J. Membr. Sci.*, 2018, **551**, 47–54.
98 S. Budhathoki, O. Ajayi, J. A. Steckel and C. E. Wilmer, *Energy Environ. Sci.*, 2019, **12**, 1255–1264.
99 G. Avci, I. Erucar and S. Keskin, *ACS Appl. Mater. Interfaces*, 2020, **12**, 41567–41579.

100 A. J. Howarth, Y. Liu, P. Li, Z. Li, T. C. Wang, J. T. Hupp and O. K. Farha, *Nat. Rev. Mater.*, 2016, **1**, 15018.
101 M. Zhai, T. Yoshioka, J. Yang, J. Wang, D. Zhang, J. Lu and Y. Zhang, *Chin. J. Chem. Eng.*, 2021, **33**, 104–111.
102 I. Erucar and S. Keskin, *J. Membr. Sci.*, 2016, **514**, 313–321.
103 Y. Yoo, Z. Lai and H.-K. Jeong, *Microporous Mesoporous Mater.*, 2009, **123**, 100–106.
104 Y. Liu, Z. Ng, E. A. Khan, H.-K. Jeong, C.-b. Ching and Z. Lai, *Microporous Mesoporous Mater.*, 2009, **118**, 296–301.
105 Y. Liu, E. Hu, E. A. Khan and Z. Lai, *J. Membr. Sci.*, 2010, **353**, 36–40.
106 X. Dong, K. Huang, S. Liu, R. Ren, W. Jin and Y. S. Lin, *J. Mater. Chem.*, 2012, **22**, 19222–19227.
107 A. Huang, Y. Chen, N. Wang, Z. Hu, J. Jiang and J. Caro, *Chem. Commun.*, 2012, **48**, 10981–10983.
108 Y. Zhang, Q. Gao, Z. Lin, T. Zhang, J. Xu, Y. Tan, W. Tian and L. Jiang, *Sci. Rep.*, 2014, **4**, 1–6.
109 D.-J. Lee, Q. Li, H. Kim and K. Lee, *Microporous Mesoporous Mater.*, 2012, **163**, 169–177.
110 A. Huang, W. Dou and J. r. Caro, *J. Am. Chem. Soc.*, 2010, **132**, 15562–15564.
111 Y. Liu, G. Zeng, Y. Pan and Z. Lai, *J. Membr. Sci.*, 2011, **379**, 46–51.
112 H. Yin, J. Wang, Z. Xie, J. Yang, J. Bai, J. Lu, Y. Zhang, D. Yin and J. Y. Lin, *Chem. Commun.*, 2014, **50**, 3699–3701.
113 M. C. McCarthy, V. Varela-Guerrero, G. V. Barnett and H.-K. Jeong, *Langmuir*, 2010, **26**, 14636–14641.
114 B. Chen, Z. Yang, Y. Zhu and Y. Xia, *J. Mater. Chem. A*, 2014, **2**, 16811–16831.
115 Y.-R. Lee, M.-S. Jang, H.-Y. Cho, H.-J. Kwon, S. Kim and W.-S. Ahn, *Chem. Eng. J.*, 2015, **271**, 276–280.
116 R. L. June, A. T. Bell and D. N. Theodorou, *J. Phys. Chem.*, 1991, **95**, 8866–8878.
117 Y. K. Ponraj and B. Borah, *J. Mol. Graphics Modell.*, 2020, **97**, 107574.
118 Z. Li, G. Xu, B. Liu, X. Lv, G. Chen, C. Sun, P. Xiao and Y. Sun, *Energies*, 2015, **8**, 11531–11545.
119 M. T. Kallo and M. J. Lennox, *Langmuir*, 2020, **36**, 13591–13600.
120 P. Krokidas, M. Castier, S. Moncho, D. N. Sredojevic, E. N. Brothers, H. T. Kwon, H.-K. Jeong, J. S. Lee and I. G. Economou, *J. Phys. Chem. C*, 2016, **120**, 8116–8124.
121 E. Garcia-Perez, P. Serra-Crespo, S. Hamad, F. Kapteijn and J. Gascon, *Phys. Chem. Chem. Phys.*, 2014, **16**, 16060–16066.
122 D. S. Chiou, H. J. Yu, T. H. Hung, Q. Lyu, C. K. Chang, J. S. Lee, L. C. Lin and D. Y. Kang, *Adv. Funct. Mater.*, 2020, 2006924.
123 N. Farzi, N. Salehi and A. Mahboubi, *Microporous Mesoporous Mater.*, 2017, **248**, 246–255.
124 B. Liu, C. Sun and G. Chen, *Chem. Eng. Sci.*, 2011, **66**, 3012–3019.
125 P. Krokidas, M. Castier and I. G. Economou, *J. Phys. Chem. C*, 2017, **121**, 17999–18011.
126 Y. Gurdal and S. Keskin, *J. Membr. Sci.*, 2016, **519**, 45–54.
127 R. C. Dutta and S. K. Bhatia, *J. Phys. Chem. C*, 2020, **124**, 594–604.
128 D. Fan, A. Ozcan, N. A. Ramsahye, D. Zhao, G. Maurin and R. Semino, *ACS Mater. Lett.*, 2021, **3**, 344–350.
129 Z. Sumer and S. Keskin, *Ind. Eng. Chem. Res.*, 2017, **56**, 8713–8722.
130 Z. Sumer and S. Keskin, *Chem. Eng. Sci.*, 2017, **164**, 108–121.
131 C. Altintas and S. Keskin, *RSC Adv.*, 2017, **7**, 52283–52295.
132 H. Kim, S. Lee and J. Kim, *Langmuir*, 2019, **35**, 3917–3924.
133 G. O. Aksu, H. Daglar, C. Altintas and S. Keskin, *J. Phys. Chem. C*, 2020, **124**, 22577–22590.
134 T. Yan, Y. Lan, M. Tong and C. Zhong, *ACS Sustainable Chem. Eng.*, 2018, **7**, 1220–1227.
135 P. Zarabadi-Poor and R. Marek, *J. Phys. Chem. C*, 2019, **123**, 3469–3475.
136 E. Haldoupis, S. Nair and D. S. Sholl, *J. Am. Chem. Soc.*, 2010, **132**, 7528–7539.
137 E. Gulcay and I. Erucar, *Ind. Eng. Chem. Res.*, 2019, **58**, 3225–3237.
138 T. Van Heest, S. L. Teich-McGoldrick, J. A. Greathouse, M. D. Allendorf and D. S. Sholl, *J. Phys. Chem. C*, 2012, **116**, 13183–13195.
139 V. A. Solanki and B. Borah, *J. Phys. Chem. C*, 2019, **123**, 17808–17822.
140 W.-q. Lin, X.-l. Xiong, H. Liang and G.-h. Chen, *ACS Appl. Mater. Interfaces*, 2021, **13**, 17998–18009.
141 W. Yang, H. Liang, F. Peng, Z. Liu, J. Liu and Z. Qiao, *Nanomaterials*, 2019, **9**, 467.
142 H. Daglar, I. Erucar and S. Keskin, *J. Membr. Sci.*, 2020, **618**, 118555.
143 C. Altintas and S. Keskin, *ACS Sustainable Chem. Eng.*, 2019, **7**, 2739–2750.
144 A. N. V. Azar, S. Velioglu and S. Keskin, *ACS Sustainable Chem. Eng.*, 2019, **7**, 9525–9536.
145 E. Besley and J. Glover, *Faraday Discuss.*, 2021, DOI: 10.1039/D1FD00005E.
146 H. Daglar and S. Keskin, *Adv. Theory Simul.*, 2019, **2**, 1900109.
147 Z. Qiao, C. Peng, J. Zhou and J. Jiang, *J. Mater. Chem. A*, 2016, **4**, 15904–15912.
148 A. P. Cote, A. I. Benin, N. W. Ockwig, M. O'Keeffe, A. J. Matzger and O. M. Yaghi, *Science*, 2005, **310**, 1166–1170.
149 D. Nazarian, J. S. Camp, Y. G. Chung, R. Q. Snurr and D. S. Sholl, *Chem. Mater.*, 2017, **29**, 2521–2528.
150 Y. Pan and Z. Lai, *Chem. Commun.*, 2011, **47**, 10275–10277.
151 I. Erucar and S. Keskin, *Chem. Eng. Sci.*, 2015, **130**, 120–128.
152 S. Keskin and D. S. Sholl, *Energy Environ. Sci.*, 2010, **3**, 343–351.
153 B. Shimekit, H. Mukhtar and T. Murugesan, *J. Membr. Sci.*, 2011, **373**, 152–159.
154 G. Dong, H. Li and V. Chen, *J. Mater. Chem. A*, 2013, **1**, 4610–4630.
155 R. Semino, J. C. Moreton, N. A. Ramsahye, S. M. Cohen and G. Maurin, *Chem. Sci.*, 2018, **9**, 315–324.
156 M. Z. Ahmad, M. Navarro, M. Lhotka, B. Zornoza, C. Téllez, W. M. de Vos, N. E. Benes, N. M. Konnertz, T. Visser and R. Semino, *J. Membr. Sci.*, 2018, **558**, 64–77.

157 R. Semino, J. P. Dürholt, R. Schmid and G. Maurin, *J. Phys. Chem. C*, 2017, **121**, 21491–21496.
158 J. Winarta, A. Meshram, F. Zhu, R. Li, H. Jafar, K. Parmar, J. Liu and B. Mu, *J. Polym. Sci.*, 2020, **58**, 2518–2546.
159 J. Olsson and G. Trägårdh, *Sep. Sci. Technol.*, 1999, **34**, 1643–1659.
160 E. Lasseuguette, R. Malpass-Evans, M. Carta, N. B. McKeown and M.-C. Ferrari, *Membranes*, 2018, **8**, 132.
161 S. A. Gülmüs and L. Yilmaz, *J. Polym. Sci., Part B: Polym. Phys.*, 2007, **45**, 3025–3033.
162 H. T. Kwon, H.-K. Jeong, A. S. Lee, H. S. An, T. Lee, E. Jang, J. S. Lee and J. Choi, *Chem. Commun.*, 2016, **52**, 11669–11672.
163 T. Kovács, S. Papp and T. Kristóf, *Condens. Matter Phys.*, 2017, **20**, 23002.
164 S.-M. Wang, Y.-X. Yu and G.-H. Gao, *J. Membr. Sci.*, 2006, **271**, 140–150.
165 A. U. Ortiz, A. Boutin, A. H. Fuchs and F.-X. Coudert, *J. Chem. Phys.*, 2013, **138**, 174703.
166 T. D. Bennett, A. K. Cheetham, A. H. Fuchs and F.-X. Coudert, *Nat. Chem.*, 2017, **9**, 11.
167 C. L. Hobday, R. J. Marshall, C. F. Murphie, J. Sotelo, T. Richards, D. R. Allan, T. Düren, F. X. Coudert, R. S. Forgan and C. A. Morrison, *Angew. Chem.*, 2016, **128**, 2447–2451.
168 A. U. Ortiz, A. Boutin, A. H. Fuchs and F.-X. Coudert, *J. Phys. Chem. Lett.*, 2013, **4**, 1861–1865.
169 P. Z. Moghadam, S. M. Rogge, A. Li, C.-M. Chow, J. Wieme, N. Moharrami, M. Aragones-Anglada, G. Conduit, D. A. Gomez-Gualdron and V. Van Speybroeck, *Matter*, 2019, **1**, 219–234.
170 S. N. Wijenayake, N. P. Panapitiya, S. H. Versteeg, C. N. Nguyen, S. Goel, K. J. Balkus, I. H. Musselman and J. P. Ferraris, *Ind. Eng. Chem. Res.*, 2013, **52**, 6991–7001.
171 A. Akbari, J. Karimi-Sabet and S. M. Ghoreishi, *Chem. Eng. Process.*, 2020, **148**, 107804.
172 S. Japip, H. Wang, Y. Xiao and T. S. Chung, *J. Membr. Sci.*, 2014, **467**, 162–174.
173 H. B. T. Jeazet, C. Staudt and C. Janiak, *Chem. Commun.*, 2012, **48**, 2140–2142.
174 M. A. Rodrigues, J. de Souza Ribeiro, E. de Souza Costa, J. L. de Miranda and H. C. Ferraz, *Sep. Purif. Technol.*, 2018, **192**, 491–500.
175 I. Pinnau and L. G. Toy, *J. Membr. Sci.*, 1996, **109**, 125–133.
176 S. Basu, A. Cano-Odena and I. F. Vankelecom, *Sep. Purif. Technol.*, 2011, **81**, 31–40.